Immunity & Ageing

RESEARCH Open Access

p16^{Ink4a}-induced senescence in cultured mast cells as a model for ageing reveals significant morphological and functional changes

Elisabeth Kleeblatt[1], Pia Lazki-Hagenbach[1], Ellon Nabet[2], Reli Cohen[2], Rajia Bahri[3], Nicholas Rogers[4], Abigail Langton[3], Silvia Bulfone-Paus[3], Dan Frenkel[2,5*] and Ronit Sagi-Eisenberg[1,5*]

Abstract

Background Mast cells (MCs) are tissue resident cells of the immune system, mainly known for their role in allergy. However, mounting evidence indicates their involvement in the pathology of age-related diseases, such as Alzheimer's disease, Parkinson's disease, and cancer. MC numbers increase in aged tissues, but how ageing affects MCs is poorly understood.

Results We show that MC ageing is associated with the increased expression of the cell cycle inhibitor p16 ^{Ink4a}, a marker and inducer of cellular senescence. Relying on this observation and the tight association of ageing with senescence, we developed a model of inducible senescence based on doxycycline-induced expression of p16^{Ink4a} in cultured bone marrow derived MCs (BMMCs). Using this model, we show that senescent MCs upregulate IL-1β, TNF-α and VEGF-A. We also demonstrate that senescence causes marked morphological changes that impact MC function. Senescent MCs are larger, contain a larger number of secretory granules (SGs) and have less membrane protrusions. Particularly striking are the changes in their SGs, reflected in a significant reduction in the number of electron dense SGs with a concomitant increase in lucent SGs containing intraluminal vesicles. The changes in SG morphology are accompanied by changes in MC degranulation, including a significant increase in receptor-triggered release of CD63-positive extracellular vesicles (EVs) and the exteriorisation of proteoglycans, as opposed to a gradual inhibition of the release of β-hexosaminidase.

Conclusions The inducible expression of p16^{Ink4a} imposes MC senescence, providing a model for tracking the autonomous changes that occur in MCs during ageing. These changes include both morphological and functional alterations. In particular, the increased release of small EVs by senescent MCs suggests an enhanced ability to modulate neighbouring cells.

Keywords Mast cells, Senescence, Ageing, p16^{Ink4a}, Secretory granules, Exosomes

*Correspondence:
Dan Frenkel
dfrenkel@tauex.tau.ac.il
Ronit Sagi-Eisenberg
histol3@tauex.tau.ac.il

Full list of author information is available at the end of the article

Background

Mast cells (MCs) are long-lived tissue resident cells of the immune system best known for their role in allergy [1, 2]. However, MCs also play physiological roles in innate immunity, acting as first-line defenders against pathogens and toxins [3], due to their strategic location at the interfaces with the external environment of tissues, such as the skin and the respiratory and digestive systems [4]. Additionally, MCs are involved in adaptive immunity against parasites and in antigen avoidance behaviour [5, 6]. However, also the pathophysiological functions of MCs extend beyond allergy. MCs have been implicated in playing a role in autoimmune diseases [7], cancer [8, 9] and neuroinflammation [10]. Though typically located next to blood vessels, MCs are also found adjacent to peripheral nerve fibers and within the brain [10, 11]. Consequently, MCs are thought to contribute to the progression of neurodegenerative diseases [12–15]. Both physiological and pathophysiological functions of MCs are mediated by the release of inflammatory mediators. Some of these mediators, such as histamine and proteases, are preformed and stored in secretory granules (SGs) and released by regulated exocytosis [16]. Others, including metabolites of arachidonic acid, cytokines, chemokines and tissue remodelling gene products, are newly synthesized by the activated MCs [17]. MCs also release extracellular vesicles (EVs), which deliver proteins, mRNA and microRNA to recipient cells, thereby influencing their microenvironment [18]. Consistent with their wide range of functions, MCs respond to multiple signals, including innate stimuli, such as bacterial products and neuropeptides [3, 19, 20], and adaptive signals, such as immunoglobulin E (IgE) class antibodies that bind to the MC FcεRI high affinity receptor. The subsequent crosslinking of cell bound IgE by cognate allergens/antigens (Ags) leads to cell activation [21].

The thin line between the physiological and pathophysiological functions of MCs likely resides in their remarkable plasticity. Depending on the type or strength of the trigger, MCs may release their SGs' content through different modes of exocytosis, leading to distinct outcomes [22]. Alternatively, MCs may release only newly synthesized inflammatory mediators without degranulation [23]. Another factor that may influence MC responses and dictate their outcomes is ageing. Ageing is associated with cellular senescence and immunosenescence, which in turn are linked with "inflammageing," a chronic inflammation prevalent in the elderly [24–26]. Given the long lifespan of MCs, it is conceivable that ageing may shift their responses from acute and protective to sustained and detrimental chronic pathophysiological responses [1]. Consistent with this premise, mounting evidence indicates the involvement of MCs in age-related disorders, including Alzheimer's and Parkinson's diseases [13, 27], cardiac fibrosis [28] and liver and kidney diseases [29, 30]. Furthermore, a clear correlation exists between ageing and increased numbers of MCs in aged tissue [11, 31, 32]. However, the precise impact of ageing on MCs remains poorly understood. Using a novel model of inducible senescence in cultured MCs as a paradigm for ageing, we demonstrate that senescent MCs acquire a proinflammatory phenotype and undergo significant morphological and functional changes including a marked increase in the regulated release of EVs.

Materials and methods

Immunofluorescence of human skin sections

Healthy, white Caucasian young (Aged 20–29 years, mean: 24.4 years ± 3.9; M = 2; F = 6) and aged (Aged 66–77 years, mean: 71.6 years ± 3.8; M = 1; F = 8) volunteers were recruited to the study. Local ethical approval was obtained from the University of Manchester Research Ethics Committee (ref. 13268, 14161, 15464 and 16099), and written informed consent was obtained from the participants. The study adhered to the principles outlined in the Declaration of Helsinki principles. Human skin biopsies were collected from the buttocks and snap-frozen in liquid nitrogen and stored at -80°C. The OCT embedded skin samples were cut into 7 µm thick cryosections and fixed with 4% formaldehyde/PBS for 25 minutes at room temperature (RT). The samples were subsequently treated with 100% methanol (10 minutes at a temperature of -20°C), blocked with 10% normal goat serum in PBS containing 0.3% Triton X-100 (v/v) for 1 hour at RT, incubated 1 hour with primary antibodies including anti-human $p16^{Ink4a}$ and anti-human tryptase, and visualized with anti-rabbit DyLight™ 594 and anti-mouse Alexa Fluor®488 (For details on the antibodies and their respective dilutions, please see Table 1). The sections were mounted using Fluoromount-G®, which contains 4',6-diamidino-2-phenylindole (DAPI) (Southern Biotech; Birmingham, USA), prior to image analysis. The images were captured using an Olympus BX53 upright microscope equipped with a 20×/0.75 UPlanS Apo objective and an Olympus DP73 camera along with Olympus CellSens v1.18 software (Evident Olympus, Tokyo, Japan). The average percentage of $p16^{+}$ MCs of each volunteer was calculated by acquiring the number of $tryptase^{+}p16^{+}$ and $tryptase^{+}p16^{-}$ cells in his/her skin sections using the cell counter tool of the extended version of ImageJ, FIJI. The results of the individuals in each group (young vs. elderly) were then averaged.

Mice and cell culture

To generate transgenic Cx3cr1Cre: rtTA-flox-flox: tet-hp16 mice, we crossed the following three lines of mice: The tet-inducible $hp16^{Ink4a}$ (tet-p16) mice (mixed C57BL/6 and 129 Sv background) [35] with the reverse

Table 1 List of purchasable antibodies used in this study

Antibody	Clone	Catalogue number	Company	Dilution
anti-CD63-PE	NVG-2	143903	Biolegend (San Diego, CA, USA)	FACS 1:200 Dot Blot 1:1000
anti-c-KIT-PE	2B8	12-1171-82	eBioscience™/ Thermo fisher (Waltham, MA, USA)	FACS 1:200
anti-FcεRI-FITCI	MAR-1	11-5898-82	Invitrogen/Thermo fisher	FACS 1:100
Goat anti Mouse-AF488	Polyclonal	A-11001	Invitrogen/Thermo fisher (Altrincham, UK)	IF 1:200
Goat anti Mouse-HRP	Polyclonal	115-035-166	Jackson ImmunoResearch Laboratories (West Grove, PA, USA)	WB 1:10000
Goat anti Rabbit-DyLight™ 594	Polyclonal	DI-1594	Vector Laboratories (Newark, CA, USA)	IF 1:200
Goat anti Rabbit-AF647	Polyclonal	ab150079	abcam	FACS 1:2000
Goat anti Rabbit-HRP	Polyclonal	115-035-003	Jackson ImmunoResearch Laboratories	WB 1:10000
Goat anti Rat-HRP	Polyclonal	A9037	Sigma Aldrich (St Louis, MO, USA)	Dot Blot 1:5000
anti-$p16^{INK4A}$	EPR1473	ab108349	Abcam (Cambridge, UK)	FACS 1:100 IF 1:400
anti-pERK 1/2	MAPK-YT	M8159	Sigma Aldrich	WB 1:10000
anti-pTyrosine	4G10	05-777	Sigma Aldrich	WB 1:1000
anti-Syntaxin-3	EPR8543	ab133750	abcam	FACS 1:100
anti-tERK 2	Polyclonal	sc-154	Santa Cruz	WB 1:1000
anti-Tryptase	AA1	369402	Biolegend (San Diego, CA, USA)	IF 1:1000

tetracycline-controlled trans-activator-flox/flox (rtTA-flox/flox) mice (C57BL6 background), kindly provided by Prof. Ittai Ben-Porath (The Hebrew University, Jerusalem, Israel), and the Cx3cr1-Cre mice (C57BL/6 background), kindly provided by Prof. Steffen Jung (The Weizmann Institute of Science, Rehovot, Israel). All mice were habituated in a 12-hour light/dark cycle and constant temperature (24±1 °C) with access to food and water *ad libitum*. The care and experimental use of all animals were performed in accordance with the Tel Aviv University guidelines and were approved by the university's animal care committee (TAU - LS - IL −2306−139–3). Bone marrow-derived MCs (BMMCs) were generated from the bone marrows obtained from hips, tibias and femurs of 8- to 10-week-old p16-inducible or control female mice. Cultures were grown in complete BMMC medium consisting of RPMI-1640 (cat # R8758, Sigma Aldrich) supplemented with 10% FBS (cat # 12657, GIBCO, Grand Island, NY, USA), 2 mM L-glutamine (cat # 03-020-1 A, Biological Industries, Beit Haemek, Israel), 0.1 mg/ml streptomycin, 100 U/ml penicillin, nystatin 12.50 U/ml (cat # 03-032-1B, Biological Industries), 1 mM sodium pyruvate (cat # 03-042-1B, Biological Industries), 10 mM HEPES (pH 7.4) (cat # 03-025-1B, Biological Industries), 57.2 pM 2-mercaptoethanol (cat # M6260, Sigma Aldrich) and 20 ng/ml IL-3 (cat # 213−13, Peprotec, Rocky Hill, NJ, USA). MC purity and functionality were confirmed by quantifying the percentage of cells that express on their surface both c-KIT and FcεRI, determined by flow cytometric analysis and by assaying the release of β-hexosaminidase in response to an IgE/Antigen trigger. Cultures of at least 90% purity and β-hexosaminidase release ≥ 20% were taken for further analyses. Cells were maintained in a humidified atmosphere of 5% CO_2 at 37 °C. Mouse peritoneal cells were isolated by intraperitoneal lavage of male C57BL/6 mice of different age as indicated. Briefly, mice were sacrificed with isoflurane inhalation followed by cervical dislocation. The peritoneal cavity was opened by a midline incision and 8 ml of sterile PMC medium [3% FBS (cat # 12657, GIBCO), 10 mM HEPES pH 7.4 (cat # 03-025-1B, Biological Industries) in PBS] were injected into the peritoneal cavity, followed by a 30 s massage of the abdomen before the fluid was collected. Peritoneal cells were collected by 5 min centrifugation of the lavage at 350 g, at 4 °C.

Cell proliferation

BMMCs were seeded at a density of 1×10^6 cells/ml in the absence or presence of 1 µg/ml DOX in complete BMMC medium. Cell number was determined using a hemacytometer and trypan blue for distinguishing live/dead cells.

MTT assay

p16 inducible BMMCs were incubated for 4 days in the absence or presence of 1 µg/ml DOX (For details on reagents, please see Table 2). 100 µl of cell suspension containing 5×10^4 cells were then seeded in 96 well plates and 10 µl of 5 mg/ml Thiazolyl Blue Tetrazolium Bromide (MTT) (M2128, Sigma Aldrich) diluted in PBS were added and the cells incubated for 3.5 h at 37 °C and 5%

Table 2 List of special reagents used in this study

Reagent	Catalogue number	Company
calcium-ionophore A23187 (Ion)	C7522	Sigma Aldrich
Albumin Dinitrophenol (DNP-HSA)	A6661	Sigma Aldrich
Doxycycline	D9891	Sigma Aldrich
Lipopolysaccharides from Escherichia coli O111:B4 (LPS)	L2630	Sigma Aldrich
Phorbol-12-myristate-13-acetate (TPA)	524400	Calbiochem (San Diego, CA, USA)

CO_2. The reaction was blocked by the addition of 110 µl of HCl 0.07 M diluted in isopropanol and the absorbance at 570 nm was measured using an absorbance microplate reader (Infinite F50; Tecan, Männedorf, Switzerland).

MC activation

For IgE-mediated activation, BMMCs were sensitized overnight with DNP-specific monoclonal IgE derived from supernatants of the hybridoma Hi-DNP-E-26.82 clone [36, 37]. Cells were washed three times in Tyrode's buffer (10 mM HEPES, pH 7.4, 130 mM NaCl, 5 mM KCl, 1.4 mM $CaCl_2$, 1 mM $MgCl_2$, 5.6 mM glucose, and 0.1% BSA), resuspended at a concentration of 1×10^6 cells/ml (except for release assays, for which 1.5×10^5 BMMCs were resuspended in a final volume of 100 µl) and triggered with 50 ng/ml DNP-HSA (Ag). For IgE-independent activation, cells were incubated with either 1 µM Ca^{2+} ionophore (A23186) and 0.1 µM TPA (Ion/TPA), or 0.5 µg/ml LPS. For measurements of degranulation cells were activated for 30 min. For Tyrosine and ERK1/2 phosphorylation, cells were activated for the indicated time periods. For mRNA expression cells were activated for 60 min. Activation by either trigger occurred at 37 °C.

β-hexosaminidase assay

β-hexosaminidase release was measured as previously described [38]. Briefly, 20 µl aliquots of supernatants and of cell lysates following cell lysis for 10 min by 100 µl of Tyrode's buffer supplemented with 0.5% Triton X-100, were incubated for 1.5 h at 37 °C with 50 µl of 1.3 mg/mL *p*-nitrophenyl-*N*-acetyl-β-D-glucosaminide in 0.1 M citrate (pH 4.5). Reactions were stopped by the addition of 180 µl of 0.2 M glycine (pH 10.7). Absorption was measured at 405 nm by using an absorbance microplate reader (Infinite F50; Tecan). Secretion is expressed as the percentage of total cellular β-hexosaminidase activity.

Transmission electron microscopy

Sample preparation and imaging

BMMCs were collected by centrifugation for 5 min at 350 g at RT and fixed in a solution containing 2.5% glutaraldehyde and 2% PFA in 0.1 M cacodylate buffer (pH 7.4) for 6 h at RT. Fixed cells were kept at 4 °C until further processing. Cells were rinsed four times for 10 min each in cacodylate buffer, postfixed, and stained with 1% osmium tetroxide, 1.5% potassium ferricyanide in 0.1 M cacodylate buffer for 1 h. Cells were then washed four times in cacodylate buffer, followed by dehydration by a series of ethanol concentrations (30%, 50%, 70%, 80%, 90%, and 95%) for 10 min at each step, followed by three washes in 100% anhydrous ethanol for 20 min each and two washes in propylene oxide for 10 min each. Following each step of dehydration, the cells were spun down for a few seconds and supernatants were removed. The cells were then infiltrated with increasing concentrations of agar 100 resin in propylene oxide (25%, 50%, 75% and 100%) for 16 h at each step. The cells were then embedded in fresh resin and polymerized in an oven at 60 °C for 48 h. Embedded cells in blocks were sectioned with a diamond knife on a Leica Reichert Ultracut S microtome (Leica Microsystems, Wetzlar, Germany), and ultrathin Sect. (80 nm) were collected onto 200-mesh thin-bar copper grids. The sections on the grids were then sequentially stained with uranyl acetate and lead citrate for 10 min each and viewed with a Tecnai 12 TEM 120 kV (Phillips, Eindhoven, the Netherlands) equipped with Phurona camera and RADIUS software (Emsis GmbH, Münster, Germany).

Image analysis

For all analyses the extended version of ImageJ, FIJI was used. Granules were classified and quantified by means of the cell counter tool. Villi were counted using the segmented line tool and a villus was only defined as such if it was connected to the cell body without leaving the focus plane. Cell area was calculated by determining the circumference of the cells using the segmented line tool and assuming a round cellular shape.

Flow cytometric analysis (FACS)

General procedures

Antibodies and dilutions used for flow cytometric analysis can be found in Table 1. For unconjugated antibodies the Goat anti Rabbit-647 (cat # ab150079, abcam) was used as a secondary antibody.

Acquisition was performed on a CytoFLEX LX flow cytometer (Beckman Coulter, Indianapolis, IN, USA). Data was analysed using the FlowJo™ Software Version 10 (Treestar, Ashland, OR, USA).

For analyses of BMMCs, a minimum of 10,000 living and/or single cells, respectively, was acquired per sample.

For analysing peritoneal MCs (PMCs), 100,000 peritoneal cells were acquired to obtain a statistically sufficient number of PMCs for analysis. Unless otherwise stated, FACS-buffer (0.5% BSA in PBS) was used for handling and analysing the FACS samples.

In analyses in which the median fluorescence intensity (MFI) was used for quantification, the MFI subtracted from the autofluorescence/fluorescence minus one/secondary only control is shown in the graphs. For analysing cell surface expression of a protein, cells were stained alive for 30 min on ice with the indicated antibodies or dyes in 3% BSA in PBS. For analysing total protein expression, cells were first fixed with 4% PFA in PBS for 15 min at RT and permeabilized with permeabilization buffer (0.1% Saponin, 5% FBS in PBS) overnight at 4 °C. Staining was performed in permeabilization buffer for 30 min RT.

In experiments in which live cells were analysed, cells were resuspended in 2 µM DAPI (cat # D9542, Sigma Aldrich) to exclude dead cells in the analysis. This approach was also used to evaluate the viability of cells in response to DOX treatment.

For staining of surface markers and total protein, the staining of the surface markers was performed on living cells prior to fixation, permeabilization and immunostaining of the intracellular target (See Table 1).

Flow cytometric measurements of degranulation

Degranulation of BMMCs was assessed by quantifying CD63 translocation to the plasma membrane, as previously described [39]. Briefly, CD63 surface expression of BMMCs was acquired and their responsiveness was evaluated by determining the percentage of CD63 positive cells. Proteoglycan exteriorisation was quantified using Avidin-Sulforhodamine, as previously described [40]. Briefly, cells were stained using 8 µg/ml Avidin-Sulforhodamine (Av.SRho) (cat # A2348, Sigma Aldrich) and the MFI of the Av.SRho was used as an indicator of surface proteoglycan.

Cell cycle analysis

For cell cycle analysis 2×10^6 BMMCs were washed three times and resuspended in ice cold PBS. Cells were subsequently fixed and permeabilized with 70% EtOH for 30 min at 4 °C. Cells were then centrifuged for 5 min at 1000 g at RT, resuspended in PBS and incubated for 15 min at RT. Cells were then centrifuged again for 10 min at 1000 g at RT, resuspended and stained with 1 µg/ml DAPI in 0.1% TritonX-100 in PBS for 30 min at RT. Flow cytometric analysis was performed, measuring the 350/405 nm excitation/emission area versus width.

RNA extraction and quantitative real-time PCR

RNA was extracted from 1.5×10^6 BMMCs using the GENEZol™ TriRNA Pure Kit+DNase (cat # GZXD100, Genaid, New Taipei City, Taiwan) according to the manufacturer's instructions. cDNA was generated using the High-Capacity cDNA Reverse Transcriptase Kit with RNase inhibitor (cat # 4374966, Thermo Fisher Scientific) conforming to the manual. The RT-qPCR was performed using SYBR-Green (cat # 4367659, Thermo Fisher Scientifics) and the StepOne™ Real-Time PCR System (Applied Biosystems, Foster City, CA, USA). Analysis was conducted using the StepOne V.2.3 software. All primers were obtained from Hylabs (Rehovot, Israel) – see Table 3. RNA expression was calculated relative to GAPDH.

Isolation of extracellular vesicles (EVs)

EVs were isolated by differential centrifugation of cell supernatants of 2×10^6 BMMCs. Cell suspensions were centrifuged for 5 min at 350 g at 4 °C to sediment the cells and the supernatants centrifuged again for 10 min at 4500 g at 4 °C to remove cell debris. EVs were then pelleted from the cleared supernatants by ultracentrifugation at 37.000 RPM (~140.000 g) for 70 min at 4 °C (Rotor: Ti70, fixed angle, cat # 337922; Centrifuge: Optima-XPN80 cat # A95765; Beckman Coulter, Indianapolis, IN, USA). EVs were washed with PBS and resuspended in 100 µl PBS.

Dot blot analysis of cellular and EV CD63

Aliquots of either EV suspensions (2 dots of 5 µl), isolated as described above, or cell lysates (1 dot of 5 µl) of BMMCs lysed for 15 min on ice in lysis buffer (50 mM HEPES [pH 7.4], 150 mM NaCl, 1 mM $MgCl_2$, 1% Triton X-100, 1 mM PMSF, protease inhibitor mixture, 2 mM Na_3VO_4) at a concentration of 3×10^6 cells/ml, were spotted on a nitrocellulose membrane. After blocking for 60 min in 5% skim milk in TBST (10 mM Tris-HCl, pH 8.0, 150 mM NaCl and 0.05% Tween-20) at RT,

Table 3 List of primers used in this study

Gene	Forward primer	Reverse primer
GAPDH	TGACCTCAACTACATGGTCTACA	CTTCCCATTCTCGGCCTTG
Lamin B1 (CAT#: MP207276 sequence origene; ordered hylabs)	AGGAAGAGCTGGAGCAGACCTA	GCAGGTTAGAGAGCTGTGAGGA
hp16	CCCAACGCACCGAATAGTTA	ACCAGCGTGTCCAGGAAG
mp16 [33]	GAACTCTTTCGGTCGTACCC	CGAATCTGCACCGTAGTTGA
IL-1β	ACCCCAAAAGATGGGCT	GATACTGCCTGCCTGAAGCTCT
TNF-α	CTGTAGCCCACGTCGTCCTAGCAA	CTGGCACCACTAGTTGGTTGTC
VEGF-A [34]	ACTGGACCCTGGCTTTACTG	TCTGCTCTCCTTCTGTCGTG

membranes were stained overnight with anti-CD63-PE in 5% BSA in TBST at 4 °C, followed by incubation with secondary HRP-conjugated Goat anti Rat antibodies for 1 h at RT. Immunoreactive dots were visualized by enhanced chemiluminescence according to standard procedures using the FUSION FX7 SPECTRA Multispectral Imaging System (Vilber, Frankfurt, Germany). Densitometry was performed using the ImageJ software.

Size and concentration analysis of EVs

Size and concentration of EVs were determined by Nanoparticle Tracking Analysis (NTA) using a Malvern Nanosight NS300 (Malvern, UK) equipped with a green (532 nm) laser and fed with a syringe pump. Each sample was diluted in sterile filtered (0.2 µm) PBS to a concentration between 5×10^7 and 2×10^8 particles/ml. After flushing the chamber thoroughly with nanopure water, the sample was fed into the Nanosight. 3–60 s videos (technical replicates) were recorded with a syringe pump speed of 20 and a camera level of 14. Videos were analysed using Malvern's internal software at a detection threshold of 5. All other settings were left as the instrument's default settings.

Cell lysis and Western blot analysis

BMMCs were lysed for 10 min on ice in lysis buffer (0.15 M sucrose, 80 mM β-glycerophosphate, 1% Triton X-100, 2 mM EDTA, 2 mM EGTA, 2 mM Na_3VO_4, 10 mM NaPPi, 1 mM PMSF and 1:25 dilution of cOmplete™ protease inhibitor cocktail (cat # 11697498001, Roche, Basal, Switzerland)) at a cell concentration of 10×10^6 cells/ml and the lysates cleared by centrifugation for 15 min at 14,000 g at 4 °C. Protein concentration was determined by the Bradford assay. Cleared lysates were then mixed with Lämmli sample buffer (1:5) and boiled for 10 min at 100 °C. Proteins were separated by 10% SDS-PAGE and gels transferred electrophoretically to nitrocellulose membranes using Trans-Blot® SD Semi-Dry Electrophoretic Transfer Cell (cat # 1703940, Bio-Rad, Hercules, CA, USA). Blots were blocked for at least 30 min in TBST containing 5% skim milk, followed by overnight incubation at 4 °C with the desired primary antibodies, three washes and subsequent incubation for 1 h at RT with HRP-conjugated secondary antibodies. Immunoreactive bands were visualized by enhanced chemiluminescence according to standard procedures using the FUSION FX7 SPECTRA Multispectral Imaging System (Vilber). Densitometry was performed using the ImageJ software.

Statistical analysis

Data was analysed using GraphPad Prism Version 8.3.0 for Windows (GraphPad Software, La Jolla, CA, USA). All data was tested for normal distribution and homoscedasticity of the comparing groups before further tests were executed. According to the resulting statistic requirements, the respective t-tests for comparing two means or ANOVA for multiple comparison were performed. All tests were two-sided. Results were considered significant when p values were smaller than 0.05. The data of each figure panel was generated from experiments which included at least 2 and up to 5 different cultures of BMMCs, derived from different mice per genotype to exclude mouse specific effects.

Results

The cell cycle inhibitor p16Ink4a is upregulated in aged MCs

Investigating the molecular changes that occur in MCs during ageing has been challenging due to difficulties in retrieving MCs from aged tissues. To address this obstacle, we leveraged the tight association between ageing and cellular senescence [41] to establish a novel model of inducible senescence in cultured MCs as a paradigm for MC ageing. Upregulation of $p16^{Ink4a}$ (herein referred to as p16), a tumour suppressor and inhibitor of the cell cycle [35, 42], has been linked with ageing and senescence [43–45]. Furthermore, induction of p16 expression has been shown to activate the hallmarks of senescence [46, 47]. Therefore, to take advantage of this property, we first investigated whether MC ageing is indeed associated with the upregulation of p16. To this purpose, we analysed the patterns of expression of p16 in peritoneal MCs (PMCs) of mice of increasing age as well as in MCs in skin derived from young and elderly donors. Staining the mouse peritoneal cells for p16 and gating for cells that are double positive for the MC markers c-KIT and the FcεRI revealed a small age-dependent increase in the incidence of PMCs (Supplementary Fig. 1). However, a strong positive correlation (Pearson $r=0.9653$) was observed between age and p16 expression, with a 5-fold increase in p16 expression in PMCs from 9-month-old mice compared to those from 2-month-old mice (Fig. 1a, b). Visualization by confocal microscopy of human skin cryosections derived from young (i.e. less than 30 years old) and elderly (i.e. older than 66) individuals, that were stained for the MC marker tryptase and for p16, demonstrated the presence of tryptase positive MCs in sections derived from either age group (Fig. 1c). However, while 12.5% of MCs, identified by their positive staining for tryptase, were also positive for p16 in sections derived from the young group, 37% of the tryptase positive MCs were p16 positive in sections derived from older skin (Fig. 1d). A significant increase in the staining for p16 was also noted in tryptase negative cells in both the dermis, most likely corresponding to skin fibroblasts, and the epidermis (Fig. 1c), consistent with the general association of upregulation of p16 with ageing.

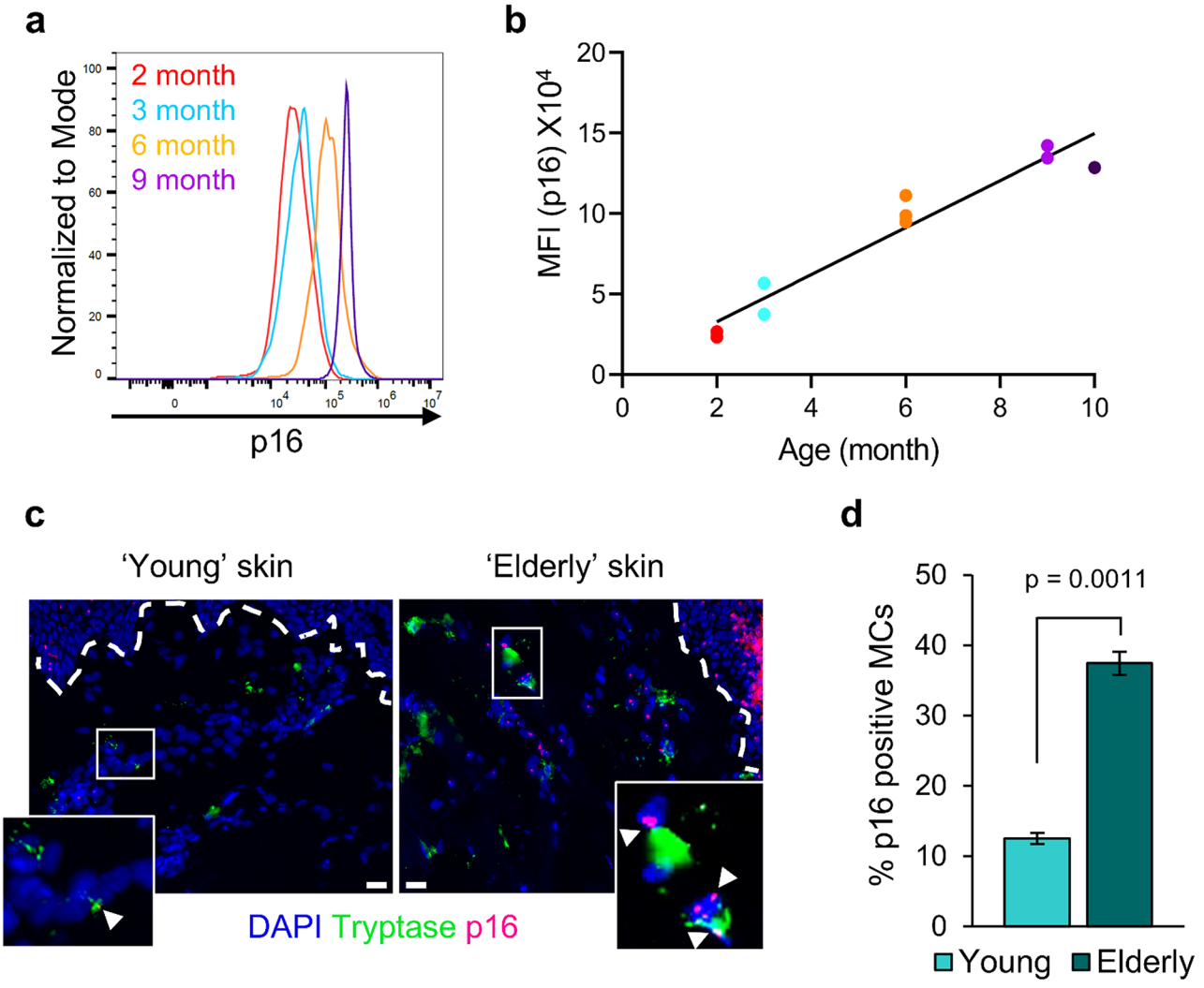

Fig. 1 p16 expression increases in "aged" MCs. **a.** Representative histograms of p16 expression by PMCs derived from mice of the indicated ages. p16 expression was monitored in FcεRI$^+$c-KIT$^+$ cells. **b.** Pearson correlation of p16 expression (MFI) and age ($r = 0.9635$, $p \leq 0.0001$). Each data point derived from flow cytometric analysis represents PMCs of a single mouse (total $n = 10$). Data was generated in two independent experiments containing mice of varying ages. **c**. Representative images of human skin sections of a young (20-year-old female) and elderly (72-year-old female) human individuals stained for the MC marker tryptase (green), for p16 (magenta) and with DAPI (blue). The dashed white line marks the border between dermis and epidermis. Scale bar = 20 µm. Insets are enlargements of the boxed areas. White arrowheads point to p16-positive MCs. **d**. Quantification of the incidence of p16 expressing skin MCs (i.e. p16$^+$tryptase$^+$ cells) of the total MC population (i.e. tryptase$^+$ cells). Population per age group is displayed. Data is presented as means ± SEM. Statistical significance was determined by Welch's t-test. $n = 8$ young and $n = 9$ elderly human individuals. Total number of analysed cells $n = 405$ young and $n = 313$ elderly

Establishing a model of inducible senescence in cultured MCs

Given the association between upregulation of p16 and MC ageing, we aimed to investigate how increased p16 expression impacts MC functions. For this purpose, we took advantage of transgenic mice that express the coding sequence of human p16 (hp16) under the control of a tetracycline (tet)-inducible promoter [35]. We chose these mice because their crossing with *Ins2*-rtTA mice successfully led to the upregulation of hp16 in pancreatic beta cells as well as induction of their senescence [35]. We crossed these mice with transgenic mice that express the Cre recombinase from the hematopoietic CX3CR1 promoter that is expressed in bone marrow derived MCs (BMMCs) [48], and with mice that have a loxP-flanked stop codon upstream of the reverse tetracycline-controlled trans-activator protein (rtTA) (Fig. 2a). Cells derived from the bone marrow of hetero- or homozygous mice for Cx3cr1-Cre, and homozygous for rtTA-flox-flox and tet-hp16, were cultured in the presence of IL-3 to allow the differentiation of hp16-inducible MCs from their bone marrow progenitors. Control cultures were derived from mice which were double negative (-/-) for at least one gene. Flow cytometric analysis of the

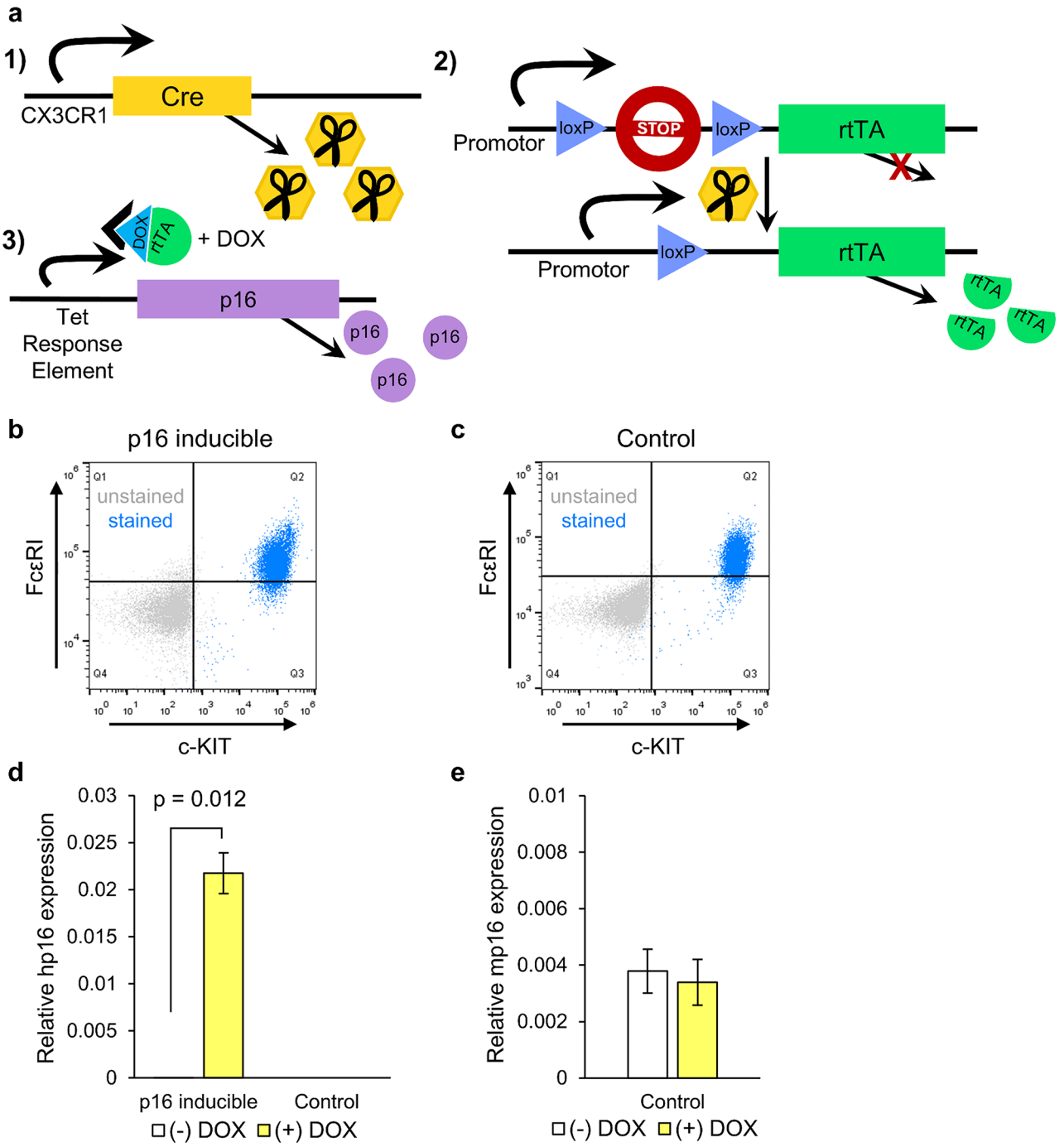

Fig. 2 Establishing a model of inducible senescence in BMMCs. **a.** A scheme of the three genetic cassettes used to generate DOX/rtTA-inducible expression of p16 in CX3CR1 expressing cells. **b**, **c**. Representative flow cytometric analyses of surface expression of c-KIT and FcεRI by BMMCs derived from p16 inducible transgenic mice (i.e. p16 inducible BMMCs, **b**) and or the transgenic control mice (i.e. control BMMCs, **c**). **d.** Expression of hp16 mRNA by p16 inducible and control BMMCs following a short-term (3 days) incubation with or without 1 µg/ml DOX. **e.** Expression of mp16 mRNA by control BMMCs following short-term incubation with or without DOX. Data is presented as means ± SEM. Statistical significance was determined using Welch's t-test (**d**) or unpaired t-test (**e**). $n = 3–8$ experiments

cells revealed the formation of an almost pure (~ 90%) population of c-KIT and FcεRI-double positive cells (Fig. 2b, c), confirming that neither the MC progenitors, nor their in vitro differentiation to MCs were affected by the transgenic genes. Exposure of the in vitro differentiated MCs (BMMCs), derived from the transgenic p16-inducible mice to 1 µg/ml of doxycycline (DOX), a concentration that was previously shown to induce genes

in BMMCs using a tetracycline-inducible system [49], led to the induction of hp16 (Fig. 2d). Importantly, incubation of the control BMMCs with DOX has neither upregulated the expression of hp16, nor did it upregulate the expression of the endogenous mouse p16 (Fig. 2d, e). We therefore used these conditions for further analyses.

Unlike BMMCs derived from control mice, which proliferated both in the absence and the presence of DOX (Fig. 3a), the number of the p16-inducible BMMCs failed to increase following DOX treatment (Fig. 3b). Staining with the DAPI viability dye excluded cell death (Fig. 3c), a notion that was supported by an MTT activity assay (Fig. 3d). These results therefore implied that the p16-inducible BMMCs stopped dividing following their DOX treatment. Indeed, analysis of their cell cycle distribution demonstrated an increase in the percentage of cells that were arrested in the G0/G1 phase, with a concomitant decrease in cells in the S and G2/M phases (Fig. 3e). No cells were detected in the sub G0/G1 phase, suggesting that DOX treatment and p16 induction do not induce apoptosis (Fig. 3e).

While the association between p16 upregulation and ageing or senescence is well established [43, 50], non-canonical functions of p16, unrelated to senescence, have also been reported [51–53]. Therefore, we examined whether p16 induction imposes cellular features commonly marked as indicators of senescence [54]. A hallmark of senescent cells is their acquisition of a pro-inflammatory phenotype. Therefore, we tested if induction of hp16 is associated with the upregulation of pro-inflammatory genes. Indeed, DOX treatment of the p16-inducible, but not the control BMMCs, upregulated the expression of IL-1β and TNF-α, as well as the expression of the angiogenic factor VEGF-A (Fig. 4a).

MCs constitutively exhibit β-galactosidase activity [55], excluding the use of this test commonly employed to identify cellular senescence. However, flow cytometric analyses revealed that DOX treatment led to an increase in the forward scatter (FSC) of the p16-inducible BMMCs, indicating an increase in their size (Fig. 4b). Finally, we also tested the effect of DOX-induced upregulation of p16 on the expression of Lamin B1, whose downregulation was noted in senescent cells [56]. Indeed, subjecting the p16-inducible, but not control BMMCs to DOX treatment significantly reduced the level of Lamin B1 expression (Fig. 4c). Therefore, based on their arrest in proliferation, decreased distribution in the S and G2/M phases of the cell cycle, upregulation of proinflammatory genes, increase in cell size and decrease in Lamin B1 expression, we conclude that the upregulation of p16 is indeed associated with the acquisition of cellular senescence by MCs.

p16-induced senescence does not affect FcεRI signalling

Flow cytometric analysis revealed that DOX treatment had no effect on the expression of c-KIT (Fig. 5a). However, a small reduction in the cell surface level of FcεRI was noted (Fig. 5b). We therefore investigated if this decrease in the surface level of FcεRI has any impact on the receptor signalling. Aggregation of the FcεRI upon the crosslinking of cell bound IgE by the appropriate antigen stimulates the phosphorylation on tyrosine residues of a number of cellular proteins by Src-like kinases [57]. Therefore, we compared the patterns of tyrosine phosphorylation induced by an IgE/antigen (IgE/Ag) trigger in p16-inducible BMMCs, in the absence or following DOX treatment. Expectedly, in the absence of DOX, sensitization of the p16-inducible BMMCs with DNP-specific IgE, followed by cell activation by the antigen, DNP-HSA, led to the tyrosine phosphorylation of cellular proteins (Fig. 5c). Focusing on proteins of 75, 40, 35 and 30 kDa, as representatives of the global phosphorylation that is induced by an IgE/Ag trigger, revealed their rapid phosphorylation since trigger exposure (Fig. 5c). A 4-day treatment with DOX prior to their IgE/Ag-trigger had no impact on the extent or kinetics of phosphorylation (Fig. 5c). Therefore, these results indicate that the FcεRI maintains its signalling in the p16-upregulated cells. This notion was further corroborated by comparing the phosphorylation patterns of the ERK1/2 MAP kinases, a later event in the cascade of signalling of the FceRI, which revealed no differences due to DOX treatment (Fig. 5d). Furthermore, IgE/Ag trigger of the p16-upregulated BMMCs led to a further increase in the expression of the proinflammatory genes (Fig. 5e), confirming their responsiveness to the cell trigger. Upregulation of IL-1β, TNF-α and VEGF-A was also noted following cell treatment with the innate trigger LPS, which activates MCs by the binding to TLR4 (Fig. 5f). Notably, though the acquisition of senescence did not affect the extent of cell responsiveness to either of these external triggers, the absolute amounts of proinflammatory transcripts in the senescent MCs were significantly larger, as compared to their levels in the activated control cells, due to the increased expression of these proinflammatory genes already under basal conditions.

p16-induced senescence increases the granularity of MCs

DOX treatment led to an increase in the sideward scatter (SSC) of the p16-inducible BMMCs, indicating an increase in their granularity (Fig. 6a). In agreement, a DOX-induced increase in the staining of the SG marker syntaxin 3 (Stx-3) [58] was also noted in the p16-inducible, but not the control BMMCs (Fig. 6b). Notably, maintaining the cells under conditions of senescence for a longer period by prolonging their incubation with DOX to one month, has further emphasized

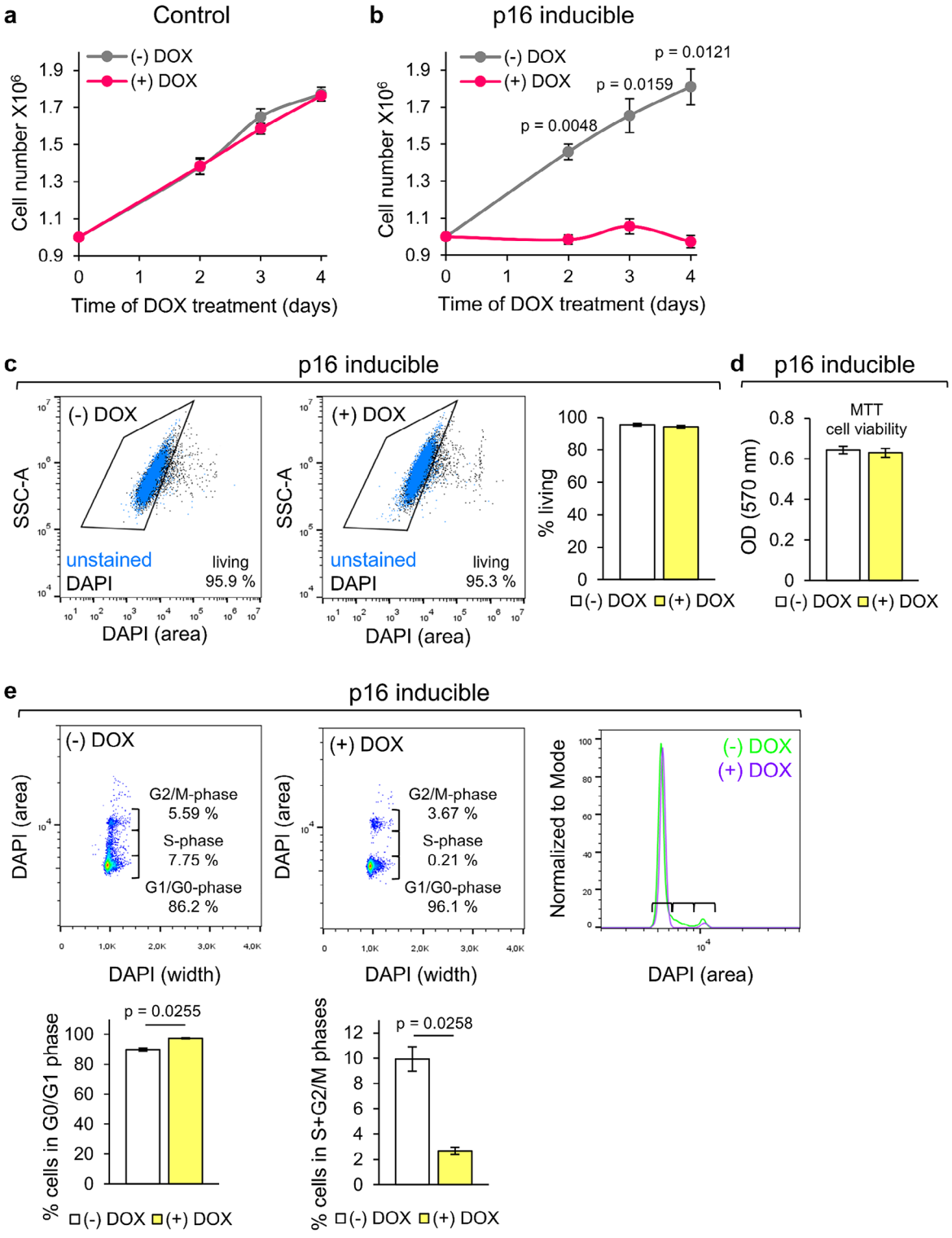

Fig. 3 Upregulation of p16 causes cell cycle arrest in BMMCs. **a**, **b.** control (**a**) and p16 inducible (**b**) BMMCs were seeded at a concentration of 1×10^6 cells/ml in the absence or presence of DOX. Cells were collected and counted at the indicated time periods. **c**. Cell viability of p16 inducible BMMCs following a 4-day incubation with or without DOX measured by quantifying the incidence of DAPI-negative cells using flow cytometry. **d.** Cell viability of 5×10^4 p16 inducible BMMCs following 4 days incubation with or without DOX and measured with an MTT assay. **e.** Representative flow cytometric analysis of the cell cycle of p16 inducible BMMCs following a 3-day incubation with or without DOX. Data is presented as means ± SEM. Statistical significance was determined by Mann-Whitney (**b**) or unpaired t-test (**a**–**e**) $n = 3$–5 experiments

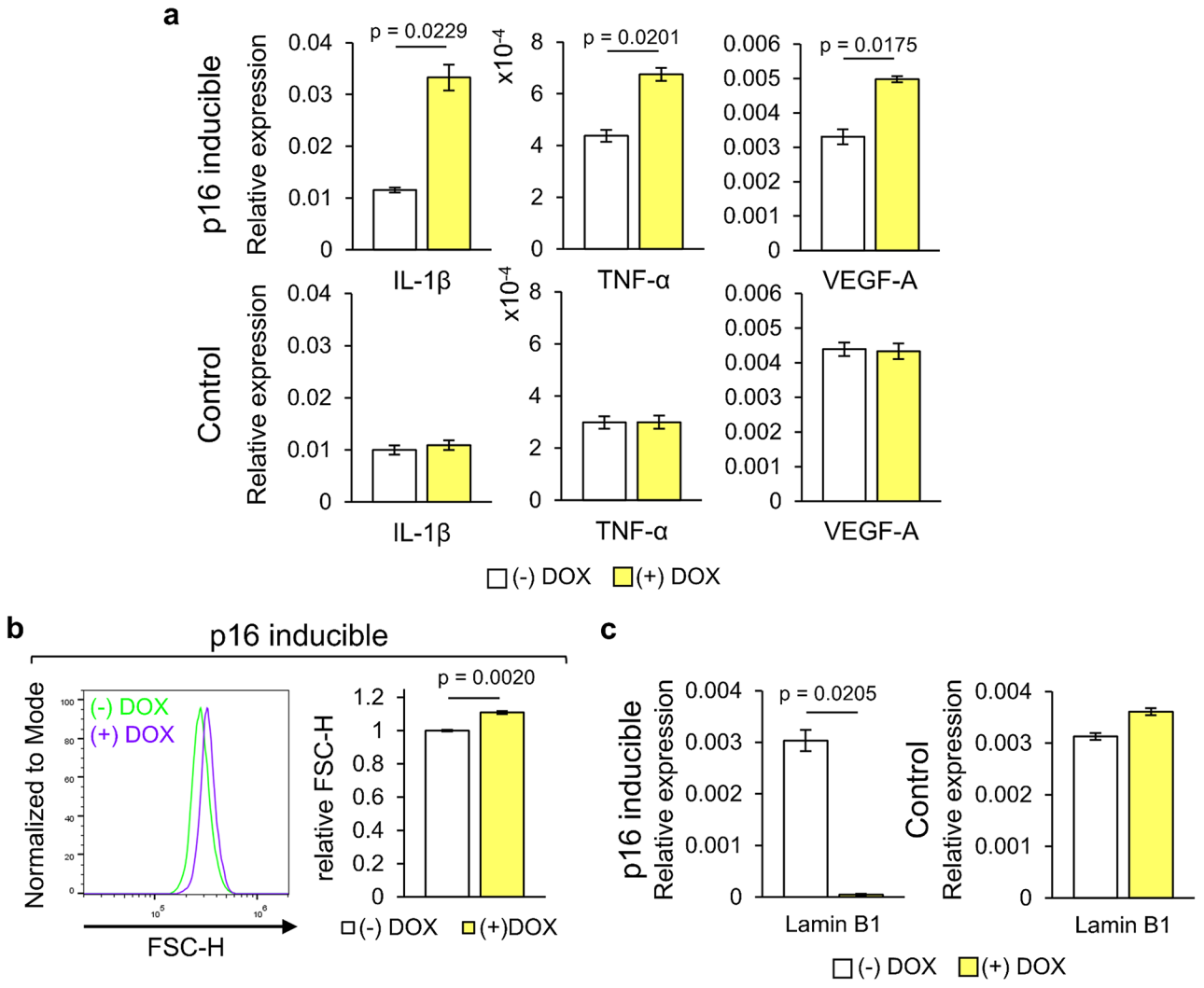

Fig. 4 The impact of p16 upregulation on gene expression and cell size. (**a**) Relative mRNA levels of IL-1β, TNF-α and VEGF-A in p16 inducible or control BMMCs after 3–4 day incubation with or without DOX. (**b**) Flow cytometric analysis of forward-scatter height (FSC-H) of p16 inducible BMMCs after 3–4 day incubation with or without DOX. (**c**) Relative mRNA levels of Lamin B1 in p16 inducible or control BMMCs after 3–4 day incubation with or without DOX. Data is presented as means ± SEM. Statistical significance was determined by Mann-Whitney (**a**), Welch's (**a**, **c**) or unpaired t-test (**a**, **b**). *n* = 3–7 experiments

their morphological changes, by increasing further their size (Fig. 6c) and granularity (Fig. 6d), which was also reflected in an increased amount of their total β-hexosaminidase, a SG resident enzyme [55] (Fig. 6e). Long-term senescence did not affect the cell viability, as indicated by their DAPI viability staining (Fig. 6f).

p16-induced senescence provokes significant changes in SG morphology

The DOX-induced increase in MC granularity prompted us to examine if senescence impacts the ultrastructure of the SGs. MC SGs are heterogenous and were previously classified based on their transmission electron microscopy (TEM) features, as Type I granules, which contain intraluminal vesicles (ILVs), reminiscent of multivesicular bodies (MVBs), Type II granules, that display an electron dense core, that is surrounded by ILVs and Type III granules, that are electron dense and lack any ILVs [59]. Consistent with this classification, inspection of either p16-inducible or control BMMCs, in the absence of prior treatment with DOX, revealed the presence of the three types of SGs (Fig. 7a), whereby approximately 40% of SGs were lucent and contained ILVs, thus conforming to Type I SGs, 40% matched the definition of Type II, and approximately 20% of SGs were electron dense, corresponding to Type III SGs (Fig. 7a, b). Strikingly, upregulation of p16 in the p16-inducible BMMCs markedly affected the SG morphology and prevalence of the distinct SG types (Fig. 7a). Low power visualization of the senescent cell suggested that the total number of SGs was

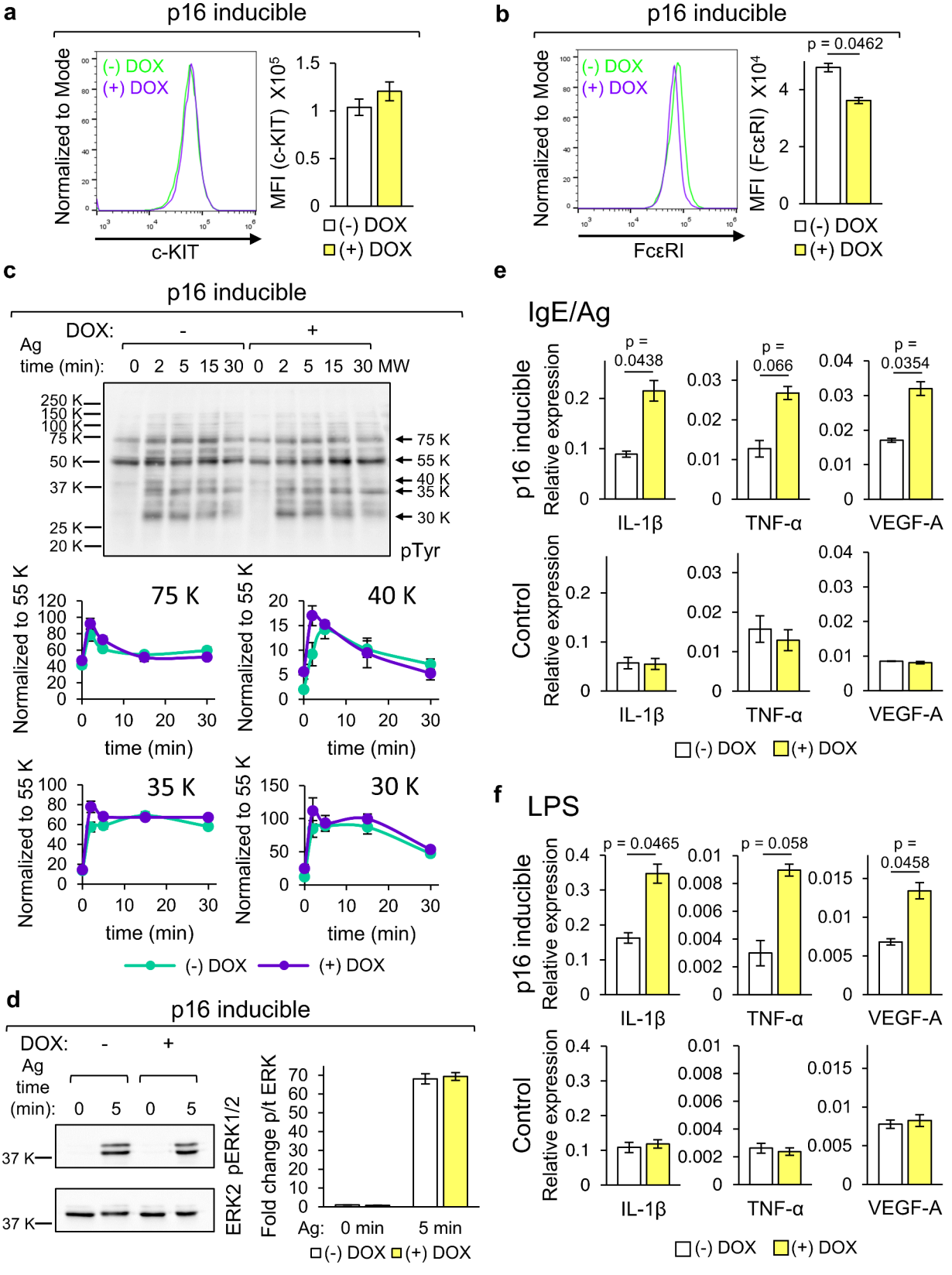

Fig. 5 (See legend on next page.)

(See figure on previous page.)

Fig. 5 The impact of p16 upregulation on MC receptor expression and responsiveness. **a**, **b.** Flow cytometric analysis of cell surface expression of c-KIT (**a**) and FcεRI (**b**) in p16 inducible BMMCs after 3–4 day incubation with or without DOX. **c**, **d.** Cell lysates derived from p16 inducible BMMCs that were triggered with IgE/Ag for the indicated time periods, following 3–4 day incubation with or without DOX, were immunoblotted using anti-phospho-Tyrosine antibodies (**c**) or anti-phospho-ERK1/2 antibodies, followed by re-probing with anti-total-ERK2 antibodies (**d**). Representative blots are shown. The intensities of the bands were quantified by densitometry. The relative pixel densities of phosphoproteins of 75, 40, 35 and 30 kDa molecular mass were normalized to the pixel density of the 55 K phosphoprotein (**c**). The ratio of phospho to total ERK2 is presented in (**d**). **e**, **f.** Relative mRNA levels of IL-1β, TNF-α and VEGF-A in p16 inducible or control BMMCs following 3–4 days incubation with or without DOX and following IgE sensitization and 1 h challenge with 50 ng/ml DNP-HSA (Ag) (**e**) or 1 h trigger with 0.5 µg/ml LPS (**f**). Data is presented as means ± SEM. $n = 3–7$ experiments. Statistical significance was determined by unpaired (**a**–**f**) and Welch's t-test (**e**)

larger (Fig. 7a). This notion was confirmed by quantitative analyses of the images (Fig. 7c), which also revealed an increase in cell size (Fig. 7d), consistent with the flow cytometric analyses. Higher resolution revealed that most SGs appeared lucent, containing either intraluminal vesicles (ILVs) and an electron-dense core, consistent with the definition of type II SGs, or clusters of dense but more amorphous material, reminiscent of type I SGs (Fig. 7a). Quantitative analysis confirmed that senescence is associated with a significant increase in type I SGs, accompanied by a significant decrease in type III SGs (Fig. 7b). Extending the senescence period to one month, which further increased MC granularity also affected further the SG morphology, leading to a greater increase in type I SGs, which was accompanied by a further decrease in type III SGs (Fig. 7a, b). Multiple SGs in the senescent cells also seemed to undergo fusion (Fig. 7a), giving rise to intracellular structures reminiscent of compound SG fusion [16]. Finally, senescence also significantly reduced the mean number of villi per cell (Fig. 7a, e). None of these changes was noted in control BMMCs that were subjected to a similar regimen of DOX treatment (Fig. 7a–e), therefore ruling out any senescence-independent effects of the drug.

p16-induced senescence differentially affects SG cargo secretion

A three-to-four-day incubation with DOX of the p16-inducible BMMCs had no effect on IgE/Ag-induced release of β-hexosaminidase (Fig. 8a), nor did it affect the translocation of CD63 to the plasma membrane (Fig. 8b), both measures of MC degranulation. However, surprisingly, quantification of the binding of Avidin Sulforhodamine (Av.SRho), which binds to glycosaminoglycans, such as heparin [60], that exteriorises during degranulation [40], demonstrated a significant increase in senescent triggered cells (Fig. 8c). Extending the period of DOX treatment to one month, conditions that markedly affected the SG morphology, led to the inhibition of the release of β-hexosaminidase in response to either IgE/Ag or a combination of Ca^{2+} ionophore and the phorbol ester TPA (Ion/TPA), that activates MCs downstream of the receptor (Fig. 8d). Therefore, these results suggest that the inhibition of degranulation was not caused by a defect in FcεRI signalling, but rather by the direct impact of p16 upregulation on the exocytic machinery. Consistent with this notion, prolonged senescence did not interfere with the upregulation of the pro-inflammatory cytokines in response to the IgE/Ag trigger (Fig. 8e).

p16-induced senescence enhances the release of small EVs

MCs constitutively release extracellular vesicles (EVs) [18]. However, cell activation by IgE/Ag enhances the release of a subset of EVs that are CD63-positive [61]. The selective impact of senescence on SG cargo release in conjunction with the increased incidence of SGs that contain ILVs therefore motivated us to investigate the influence of p16-imposed senescence on the regulated release of EVs. Consistent with the previous report [61], IgE/Ag stimulated the release of CD63-positive EVs by either control or p16-inducible BMMCs (Fig. 9a). However, DOX treatment selectively increased the amount of CD63 released by triggered p16-inducible BMMCs, but not by their control counterparts (Fig. 9a). The increase in released CD63 following DOX treatment of p16-inducible BMMCs may indicate an elevated EV release. Alternatively, senescence could result in increased CD63 expression, thereby leading to a higher content of CD63 in the released EVs. To distinguish between the effect of senescence on the amount of CD63 expressed in EVs and its effect on the number of EVs, we examined the impact of DOX on the total amount of CD63 in p16-inducible BMMCs and have also quantified the concentration of the released EVs using nanoparticle tracking analysis (NTA). Subjection of the p16-inducible BMMCs to a 4-day treatment with DOX led to a small (37%) increase in CD63 expression (Fig. 9b), which could however not account for the 2.5-fold increase in the released CD63. Also, the NTA detected only a small increase in the total number of EVs released in response to the IgE/Ag trigger by senescent cells that was not statistically significant (Fig. 9c). However, a striking effect of p16-induced senescence was noted on the size distribution of the released EVs. While the majority of EVs released by non-senescent cells ranged between 150 and 300 nm, consistent with the size of EVs released by BMMCs in response to an Ion/TPA trigger [62], the majority of EVs released by senescent MCs ranged between 30 and 150 nm (Fig. 9d). MCs release both CD63-positive microvesicles and CD63-positive exosomes [62, 63]. However, based on their size,

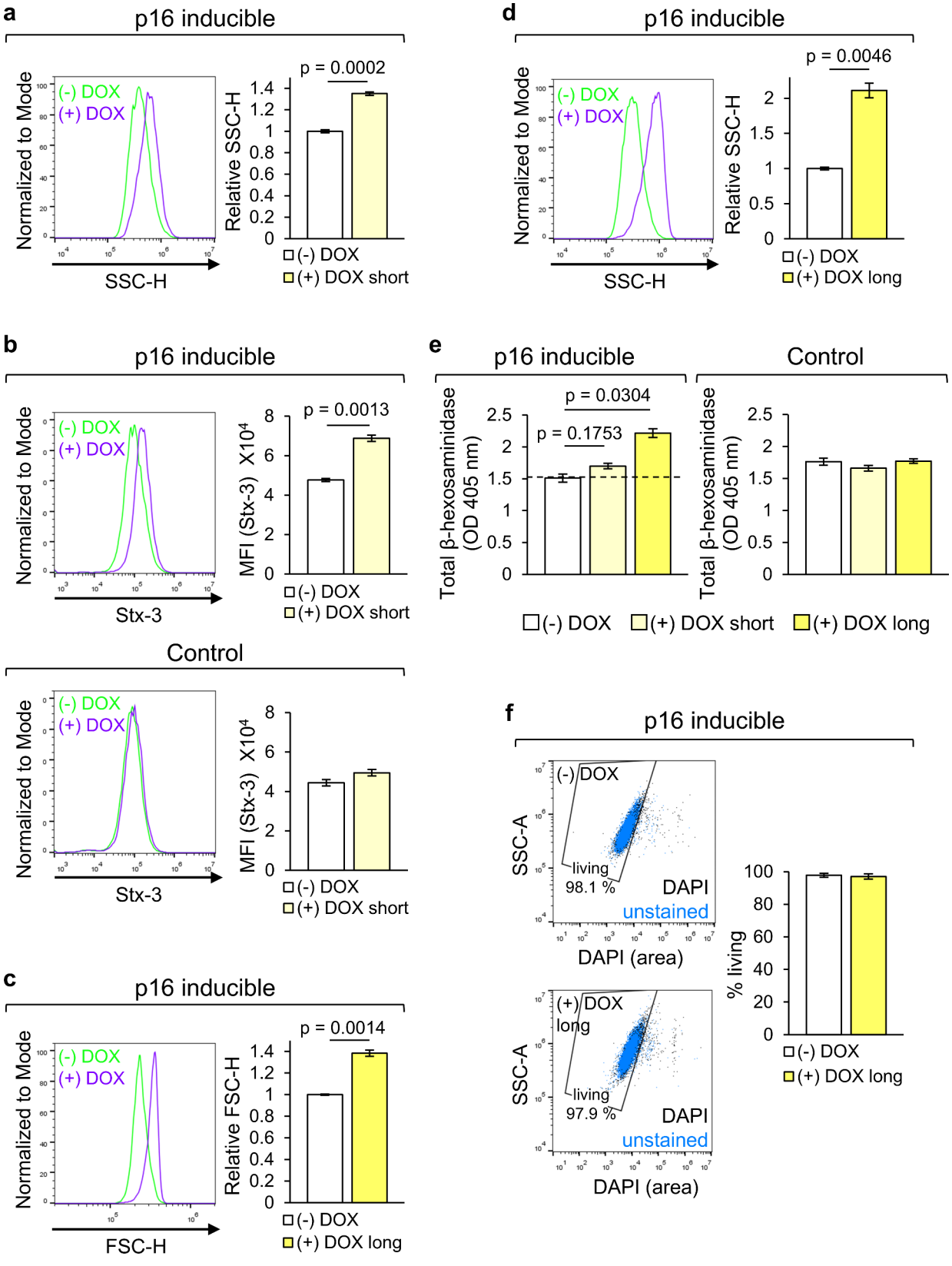

Fig. 6 (See legend on next page.)

(See figure on previous page.)

Fig. 6 Senescence increases MC granularity. (**a**) Flow cytometric analysis of sideward scatter height (SSC-H) of p16 inducible BMMCs after short-term (3–4 days) incubation with or without DOX. (**b**) Flow cytometric analysis of Stx-3 expression in p16 inducible and control BMMCs following short-term incubation with or without DOX. **c**, **d.** Flow cytometric analysis of FSC-H (**c**) and SSC-H (**d**) of p16 inducible BMMCs after long-term (one month) incubation with or without DOX. **e.** Total β-hexosaminidase activity of p16 inducible and control BMMCs following short- or long-term incubation with or without DOX. **f.** Cell viability of p16 inducible BMMCs following long-term incubation with or without DOX measured by quantifying the incidence of DAPI-negative cells using flow cytometry. Data is presented as means ± SEM. Statistical significance was determined by unpaired t-test (**a**–**d**, **f**) or Brown-Forsythe and Welch ANOVA tests with post hoc Dunnett's T3 multiple comparisons test (**e**). $n = 3–7$ experiments

the detected increase in ILV-containing SGs, and their regulated release, we reckon that senescence is associated with an increase in the release of SG-derived exosomes, though the distinction between exosomes and small ectosomes that bud directly from the plasma membrane requires further investigation. In any event, the increase in the amount of released CD63 implies its higher content in the subset of small EVs whose IgE/Ag-induced release is enhanced by senescence.

Discussion

An increase in MC numbers with age has been noted in multiple organs, including the skin [11, 64], mesenteric lymphatic vessels [65], the gut [32], the brain [32], and the liver [66]. Additionally, MCs change their position in aged skin from close proximity to blood vessels to the vicinity of macrophages and nerves [11]. Age-dependent changes in their functions have also been observed, including a block in their ability to degranulate in aged skin [11] and reduced responsiveness to stimuli in aged mesenteric lymphatic vessels [65]. Age-related alterations in MC functions have been implicated in playing a role in liver fibrosis [66] and neurodegenerative diseases, such as Alzheimer's disease [14]. However, the precise changes that occur in aged MCs remained largely unresolved. Leaning on the close association between ageing and cellular senescence, we have set up a novel model of inducible senescence in cultured BMMCs. This model enables continuous and molecular-level tracking of autonomous changes in MCs during ageing, and could provide the basis for future analyses of the impact of ageing on MC crosstalk with their microenvironment, a crosstalk that has been implicated in tumour progression [9], neurodegeneration [14], and the modulation of immune responses [67–69]. We based our model on the inducible upregulation of the cell cycle inhibitor p16, which we show is upregulated in both human MCs of aged skin and peritoneal MCs of aged mice. That upregulation of p16 indeed leads to MC senescence was validated by our findings demonstrating the association of upregulation of p16 with a combination of senescence markers, including the arrest of proliferation, downregulation of Lamin B1, upregulation of pro-inflammatory genes, including IL-1β, TNF-α and VEGF-A, and an increase in cell size, all of which are known features of senescent cells [70–72]. Therefore, although p16 has multiple functions that are unrelated to senescence or ageing [54], the induction of a combination of senescence markers in the p16-upregulated MCs, strongly suggests their acquisition of senescence.

Characterization of the senescent MCs has highlighted alterations in both their morphology and function, suggesting a direct link between ageing and changes in MC functions. In particular, p16-induced senescence was associated with an upregulation of proinflammatory genes and an increase in both the cell size and granularity. In this context, it is interesting to note that transformation of murine peritoneal MCs, which occurred due to the spontaneous loss of *Cdkn2a/Arf* (encoding murine p14 and p16), resulted in a significant decrease in their granularity and size compared to primary MCs [73], thus opposite to the phenotype of the p16-upregulated senescent MCs. Therefore, taken together, these results indicate an association between cell cycle progression and MC size and granularity. Ultrastructural analysis of the senescent MCs revealed that these cells are not only larger but also have a significantly lower number of surface villi. Although the functional implications of the reduction in plasma membrane protrusions are presently unknown, it is conceivable that such changes may have important effects on MC communication with other cells. Plasma membrane protrusions play a role in cell migration [74], so their reduced number may hamper MC mobility. Nevertheless, as noted above, MC numbers are increased in ageing tissues, possibly due to the increased release of cytokines and chemotactic factors by the MCs and their senescent environment leading to the increased recruitment of immature MCs and prolonged survival. Alternatively, the decrease in villi may impact the MC's ability to leave the area of inflammation, when no longer needed. Further, the decrease in the number of villi may affect the MC macropinocytic activity, which mediates their uptake of external material and the internalization of cell surface receptors such as MRGPRX2 [75], thereby influencing MC responsiveness to certain ligands.

A second and most striking alteration is the change in the number and morphology of the SGs, and the differential impact on their cargo release. Specifically, the increase in SG number is associated with an increase in the number of lucent SGs that also contain ILVs, while the number of electron dense SGs is reduced. We have recently demonstrated that MC SGs acquire their ILVs and capacity to release exosomes by their fusion with

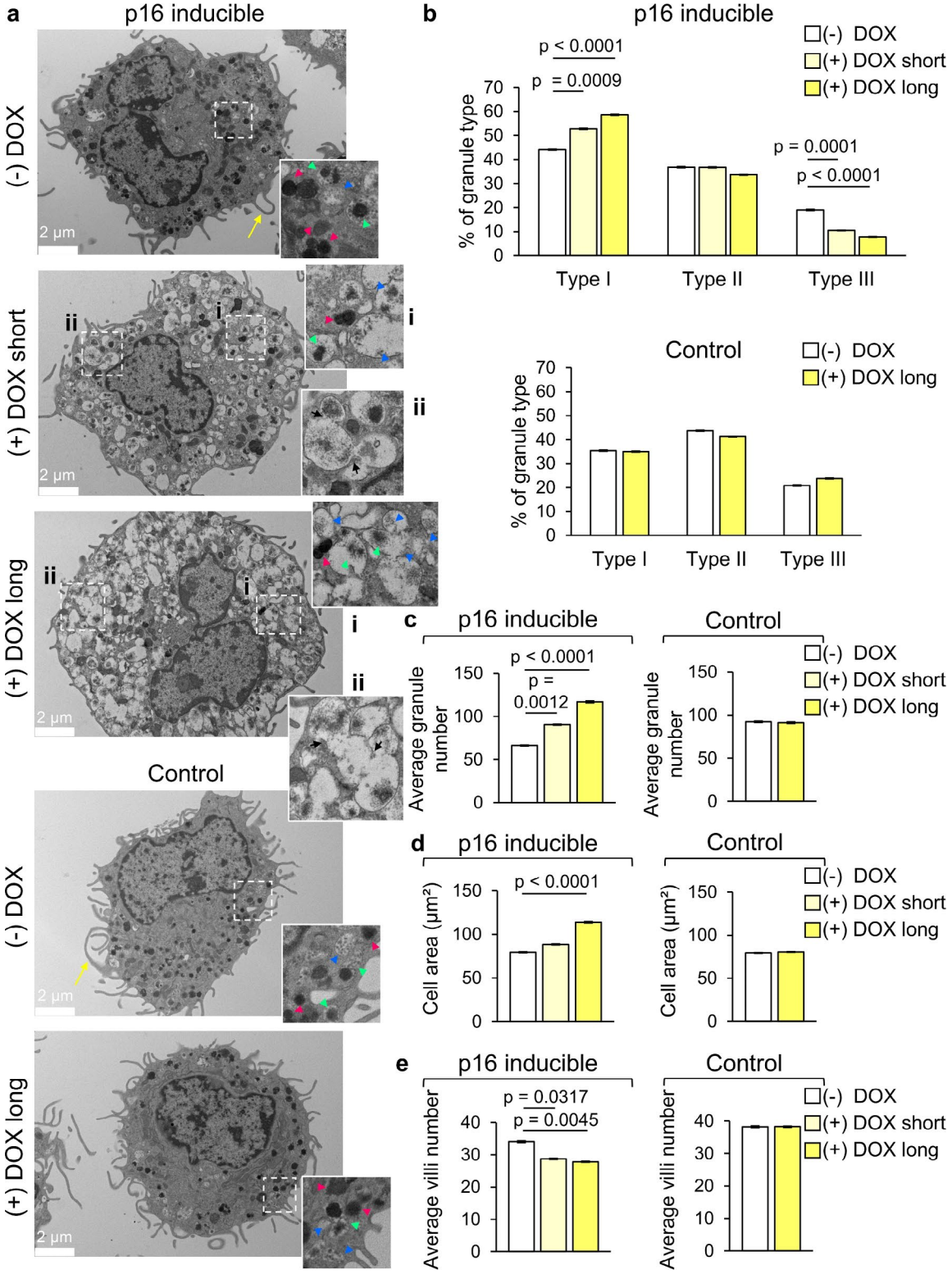

Fig. 7 Senescence affects SG morphology. **a.** TEM images of p16 inducible and control BMMCs after short- or long-term incubation with or without DOX. Scale bar = 2 µm. Insets are enlargements of the boxed areas. Arrow heads indicate the granule types: Blue = ILV containing type I; green = mixed ILV and dense cores containing type II; pink = electron dense core type III. Yellow arrows point to sites of macropinocytic cup formation. Black arrows point to sites of SG fusion. **b–e.** Quantification of the incidence of granule type per cell (**b**), average granule number (**c**), cell area (**d**) and average number of villi per cell (**e**) following short or long-term incubation with or without DOX. Data is presented as means ± SEM. Statistical significance was determined by Kruskal-Wallis test with post hoc Dunn's multiple comparison test. *n* = 37–52 cells per condition

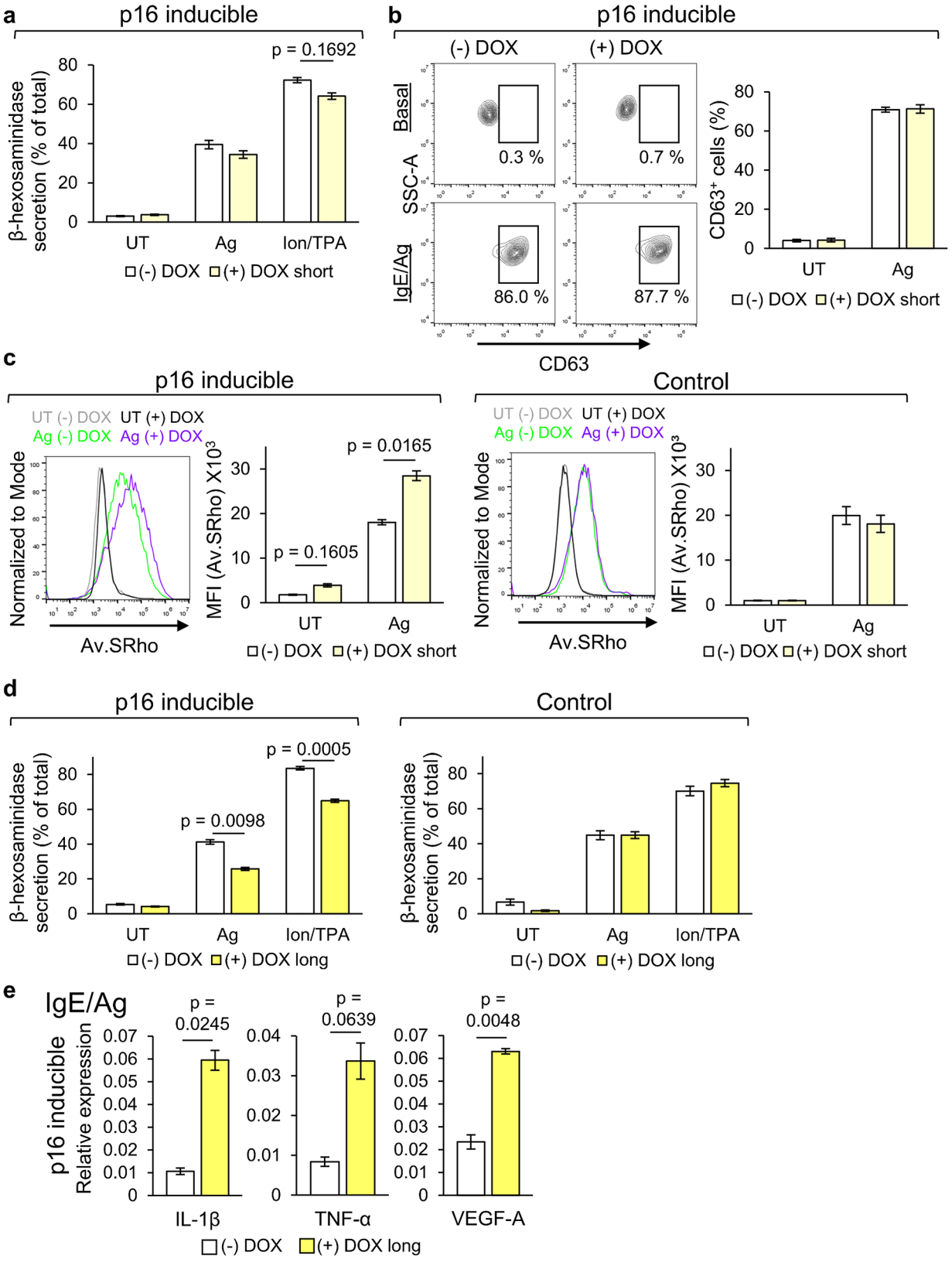

Fig. 8 (See legend on next page.)

(See figure on previous page.)

Fig. 8 Senescence impacts SG cargo release distinctly. (**a**) β-hexosaminidase release of p16 inducible BMMCs in response to IgE/Ag or Ion/TPA, following short-term incubation with or without DOX. Release is presented as percentage of total β-hexosaminidase. (**b**) Cell surface expression of CD63 in untreated (UT) or IgE/Ag-activated p16 inducible BMMCs following short-term incubation with or without DOX. (**c**) Proteoglycans exteriorisation assayed by flow cytometric analysis of Av.SRho binding to untreated or IgE/Ag-activated p16 inducible or control BMMCs following short-term incubation with or without DOX. (**d**) IgE/Ag or Ion/TPA-induced β-hexosaminidase release by p16 inducible or control BMMCs after long-term incubation with or without DOX. (**e**) Relative mRNA levels of IL-1β, TNF-α and VEGF-A in IgE/Ag-activated p16 inducible BMMCs following long-term incubation with or without DOX. Data is presented as means ± SEM. Statistical significance was determined by either Mann-Whitney (**c**), Welch's (**d**) or unpaired t-test (**a–e**). $n = 3–10$ experiments

amphisomes [76]. Therefore, the senescence related increase in ILV-containing SGs at the expense of a decrease in their ILV-deficient SGs (i.e. type III) implies an age-dependent increase in SG fusion events with the endocytic/autophagic system. This notion is consistent with the decrease in lysosomal activity, which occurs during ageing [77, 78] leading to the accumulation of amphisomes [79], which in turn may lead to an increase in the incidence of amphisome fusion with the SGs. Indeed, while non-senescent BMMCs release in response to an IgE/Ag trigger a mixed population of small EVs, whose sizes ranged between 100 and 300 nm, senescent cells release a more homogenous population of small EVs, which though not directly proven, comply to exosomes based on their size and association with an increased number of ILV-containing SGs. In this context, it is interesting to note that synthetic triggering of BMMCs, by the combination of a Ca^{2+} ionophore and the phorbol ester TPA, was recently shown to enhance the release of medium sized EVs, whose sizes range between 200 and 400 nm, while the release of larger EVs (i.e. 2000 nm) is suppressed [62]. These results are consistent with our findings on the release of small to medium EVs in response to an allergic, IgE/Ag trigger. However, we show that senescence and ageing are linked with a shift of the EV population towards the release of small EVs which are enriched in CD63, likely reflecting their common amphisomal source. Whether this subpopulation of small EVs carries unique cargo whose uptake by recipient cells contributes to inflammageing is presently unknown. MCs release a wide spectrum of biologically active mediators, accounting for their immense impact on their environment, that by far exceeds their number in the tissue. Given the critical role played by EVs in intercellular communication, our results strongly suggest that ageing increases even further their influence. Moreover, considering the increased expression of inflammatory genes in senescent MCs, it is envisioned that the ability of MCs to instigate a pro-inflammatory environment increases with ageing, aligning with their documented involvement in age-related diseases. Interestingly, under the same conditions, the binding of Av.SRho to activated MCs also increases, suggesting an increase in the exteriorisation of proteoglycans, such as heparin, by the triggered senescent cells, though no change is detected in the release of β-hexosaminidase or the translocation of CD63 to the plasma membrane. The reason for this discrepancy is presently unknown. MCs release their SG contents by distinct modes of exocytosis, including kiss-and-run exocytosis, that leads to a partial and selective release of SG cargo, and full or compound exocytosis which allow the full discharge of the SGs' contents [22]. Therefore, the acquisition of ILVs may increase the incidence of compound exocytosis leading to increased exteriorisation of proteoglycans alongside the increase in the release of exosomes. Our EM analyses demonstrate an increase in fused SGs in the senescent MCs, which is consistent with our recent findings that fusion with amphisomes not only imparts to the SGs their capacity to release exosomes but also generates hubs for the fusion of multiple individual SGs [76]. However, whether their presence reflects or facilitates their compound exocytosis in response to cell trigger awaits future investigations. We also show that prolonged senescence hinders the capacity of MCs to release β-hexosaminidase. This inhibition is not due to a defect in the enzyme's production, as the cellular amount of active β-hexosaminidase does increase. Moreover, it is not a senescence-independent effect of DOX, as no inhibition was observed in control BMMCs treated with the same concentration of DOX for the same period. Though we cannot exclude the possibility that the reduction in the release of β-hexosaminidase is due to its increased association with the endocytic/lysosomal system rather than with the SGs, our recent findings demonstrating the fusion between the SGs and amphisomes [76], in conjunction with our observation of less degranulated MCs in aged skin [11], strongly suggest that senescence indeed interferes with MC degranulation. The SGs appear more lucent following prolonged senescence, which leads us to speculate that prolonged senescence may induce piecemeal degranulation (PMD), whereby SG contents are partially released via vesicles that bud off the SG. PMD may thus result in the partial emptying of SGs, accounting for their lucent appearance and it may also interfere with the triggered release of β-hexosaminidase by exocytosis. PMD has been associated with chronic inflammation and may thus further contribute to MC-dependent inflammageing.

Conclusions

In this study we show that MC ageing is associated with the upregulation of p16 and that the induction of p16 expression leads to cellular senescence, thus providing a model for ageing. We show that senescent MCs undergo

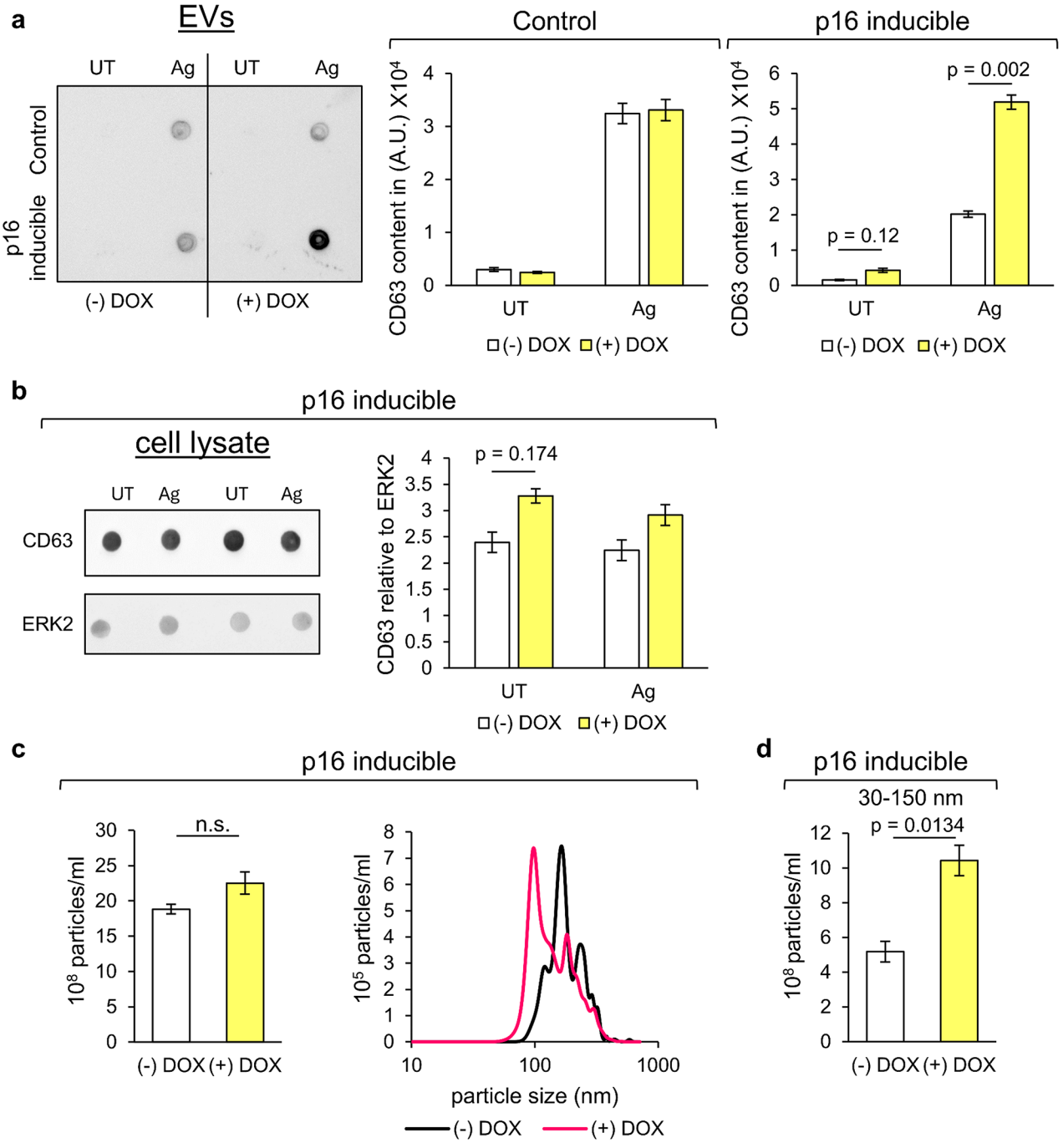

Fig. 9 Senescence enhances regulated release of small CD63-positive EVs. (**a**) Representative dot blot and densitometric quantification of EVs released by untreated (UT) or IgE/Ag-activated 2×10^6 p16 inducible or control BMMCs following a short-term incubation with or without DOX and staining for CD63. (**b**) Representative dot blots and densitometric quantification of cell lysates of UT or IgE/Ag-activated p16 inducible BMMCs following a short-term incubation with or without DOX and staining for CD63 and with anti-total ERK2 for normalization. **c**, **d.** Nanoparticle Tracking Analysis of EVs' concentration and size (**c**) or concentration of 30–150 nm sized EVs (**d**) released by 2×10^6 IgE/Ag-triggered p16 inducible BMMCs following a short-term incubation with or without DOX. Data is presented as means ± SEM. Statistical significance was determined by either Welch's (**a**) or (un)paired t-test (**a**–**d**). $n = 3$–5 experiments

marked changes in their morphology and function. Specifically, ageing is linked with the acquisition of a proinflammatory phenotype, a gradual inhibition of the release of β-hexosaminidase and an increase in the exteriorisation of heparin concomitantly to a significant increase in the regulated release of small CD63-positive exosomes. These changes are likely to impact the MC crosstalk with their microenvironment and contribute to a chronic inflammation linked with disease.

Abbreviations

MC	Mast cell
SG	Secretory granule
IgE	Immunoglobulin E
FcεRI	High-affinity receptors for IgE
IgE/Ag	IgE/Antigen
Ion	Calcium ionophore
TPA	12-O- tetradecanoylphorbol-13-acetate
LPS	Lipopolysaccharides from Escherichia coli
rTA	Tetracycline reverse transcriptional activator

Supplementary Information

The online version contains supplementary material available at https://doi.org/10.1186/s12979-024-00478-5.

Supplementary Material 1: Figure 1 quantification of the incidence of PMCs of mice different ages**(a)** Flow cytometric gating strategy showing the SSC-H/FSC-H distribution of fixed permeabilized peritoneal cells in the first gate and FcεRI/c-KIT-stained peritoneal cells in the second gate allowing the identification of PMCs exclusively expressing both markers. **(b)** Pearson correlation of the incidence of PMCs ($FcεRI^+c\text{-}KIT^+$ cells) in the peritoneal cell population with age ($r = 0.6567$, $p = 0.0391$). Each data point (circle or star) represents the incidence of PMCs of a single mouse (total $n = 10$). Data was generated in two independent experiments containing mice of varying ages.

Acknowledgements

The authors would like to thank Dr. Yael Friedman, The Hebrew University, for her help in the electron microscopy studies. The authors also thank Poonam Halai and Orsolya Kiss for their technical help and Prof. Ittai Ben-Porath and Prof. Prof. Steffen Jung for their generous gift of mice. This study was funded by the Ministry of Science and Technology (grant number 3-15715 to RSE and DF) and by the Israel Science Foundation, founded by the Israel Academy for Sciences (grant number 1600/19 to RSE), and scholarships by the Prajs-Drimmer Institute for development of Anti-Degenerative Drugs and by the Healthy Longevity Research Center, Tel Aviv University (to EK).

Author contributions

R.S-E. and D.F. conceived the project, analysed the data, discussed the results and acquired funding. E.K. designed and performed the experiments, analysed the data, discussed the results and wrote the original draft commented on the manuscript. P.L-H. isolated and performed the experiments on murine peritoneal cells and analysed the data. E.N. and R.L. maintained and genotyped the transgenic mice. R. B. immunostained the skin sections. N.R. performed the NTA analyses. A.L. recruited the volunteers. S. B-P. supervised the human skin analyses. R.S-E. wrote the manuscript. All authors reviewed and commented on the manuscript.

Data availability

No datasets were generated or analysed during the current study.

Declarations

Competing interests

The authors declare no competing interests.

Author details

[1]Department of Cell and Developmental Biology, Faculty of Medical and Health Sciences, Tel Aviv University, Tel Aviv 69978, Israel
[2]Department of Neurobiology, School of Neurobiology, Biochemistry and Biophysics, Faculty of Life Sciences, Tel Aviv University, Tel Aviv 69978, Israel
[3]Lydia Becker Institute of Immunology and Inflammation, Division of Musculoskeletal and Dermatological Sciences, School of Biological Sciences, Faculty of Biology, Medicine and Health, The University of Manchester, Manchester M13 9PT, UK
[4]Department of Environmental Studies, School of Mechanical Engineering, Tel Aviv University, Tel Aviv 69978, Israel
[5]Sagol School of Neuroscience, Tel Aviv University, Tel Aviv 69978, Israel

Received: 20 July 2024 / Accepted: 14 October 2024
Published online: 11 November 2024

References

1. Kiernan JA. Production and life span of cutaneous mast cells in young rats. J Anat. 1979;128(Pt 2):225–38.
2. Riley JF, West GB. Histamine in tissue mast cells. J Physiol. 1952;117(4):P72–3.
3. Dahlin JS, Maurer M, Metcalfe DD, Pejler G, Sagi-Eisenberg R, Nilsson G. The ingenious mast cell: contemporary insights into mast cell behavior and function. Allergy. 2021;77(1):83–99.
4. da Silva EZM, Jamur MC, Oliver C. Mast cell function. J Histochem Cytochemistry. 2014;62(10):698–738.
5. Plum T, Binzberger R, Thiele R, Shang F, Postrach D, Fung C, et al. Mast cells link immune sensing to antigen-avoidance behaviour. Nature. 2023;620(7974):634–42.
6. Wilainam P, Nintasen R, Viriyavejakul P. Mast cell activation in the skin of Plasmodium Falciparum malaria patients. Malar J. 2015;14(1).
7. Walker ME, Hatfield JK, Brown MA. New insights into the role of mast cells in autoimmunity: evidence for a common mechanism of action? Biochim Biophys Acta. 2012;1822(1):57–65.
8. Aponte-López A, Muñoz-Cruz S. Mast cells in the tumor microenvironment. Adv Exp Med Biol. 2020;1273:159–73.
9. Gorzalczany Y, Merimsky O, Sagi-Eisenberg R. Mast cells are directly activated by Cancer cell–derived extracellular vesicles by a CD73- and adenosine-dependent mechanism. Translational Oncol. 2019;12(12):1549–56.
10. Mittal A, Sagi V, Gupta M, Gupta K. Mast cell neural interactions in Health and Disease. Front Cell Neurosci. 2019;13.
11. Pilkington SM, Barron MJ, Watson REB, Griffiths CEM, Bulfone-Paus S. Aged human skin accumulates mast cells with altered functionality that localize to macrophages and vasoactive intestinal peptide-positive nerve fibres. Br J Dermatol. 2018;180(4):849–58.
12. Hendriksen E, van Bergeijk D, Oosting RS, Redegeld FA. Mast cells in neuroinflammation and brain disorders. Neurosci Biobehavioral Reviews. 2017;79:119–33.
13. Lin C-CJ, Herisson F, Le H, Jaafar N, Chetal K, Oram MK et al. Mast cell deficiency improves cognition and enhances disease-associated microglia in 5XFAD mice. Cell Rep. 2023;42(9).
14. Jones MK, Nair A, Gupta M. Mast cells in neurodegenerative disease. Front Cell Neurosci. 2019;13.
15. Martínez-Gopar PE, Pérez-Rodríguez MJ, Rodríguez-Manzo G, Garduño-Gutierrez R, Tristán-López L, Angeles-López QD, et al. Mast cells and histamine are involved in the neuronal damage observed in a quinolinic acid-induced model of Huntington's disease. J Neurochem. 2021;160(2):256–70.
16. Moon TC, Befus AD, Kulka M. Mast cell mediators: their differential release and the secretory pathways involved. Front Immunol. 2014;5.
17. Mukai K, Tsai M, Saito H, Galli SJ. Mast cells as sources of cytokines, chemokines, and growth factors. Immunol Rev. 2018;282(1):121–50.
18. Lecce M, Molfetta R, Milito ND, Santoni A, Paolini R. FcεRI Signaling in the modulation of allergic response: role of mast cell-derived exosomes. Int J Mol Sci. 2020;21(15).
19. Green DP, Limjunyawong N, Gour N, Pundir P, Dong X. A mast-cell-specific receptor mediates neurogenic inflammation and Pain. Neuron. 2019;101(3):412–e203.
20. Trivedi NH, Guentzel MN, Rodriguez AR, Yu J-J, Forsthuber TG, Arulanandam BP. Mast cells: multitalented facilitators of protection against bacterial pathogens. Expert Rev Clin Immunol. 2014;9(2):129–38.

21. Nagata Y, Suzuki R, FcεRI:. A Master Regulator of mast cell functions. Cells. 2022;11(4).
22. Gaudenzio N, Sibilano R, Marichal T, Starkl P, Reber LL, Cenac N, et al. Different activation signals induce distinct mast cell degranulation strategies. J Clin Invest. 2016;126(10):3981–98.
23. Supajatura V, Ushio H, Nakao A, Okumura K, Ra C, Ogawa H. Protective roles of mast cells against enterobacterial infection are mediated by toll-like receptor 4. J Immunol. 2001;167(4):2250–6.
24. Lee K-A, Flores RR, Jang IH, Saathoff A, Robbins PD. Immune Senescence, Immunosenescence and Aging. Front Aging. 2022;3.
25. Liu Z, Liang Q, Ren Y, Guo C, Ge X, Wang L et al. Immunosenescence: molecular mechanisms and diseases. Signal Transduct Target Therapy. 2023;8(1).
26. Ferrucci L, Fabbri E. Inflammageing: chronic inflammation in ageing, cardiovascular disease, and frailty. Nat Reviews Cardiol. 2018;15(9):505–22.
27. Kempuraj D, Thangavel R, Fattal R, Pattani S, Yang E, Zaheer S, et al. Mast cells release chemokine CCL2 in response to Parkinsonian Toxin 1-Methyl-4-phenyl-pyridinium (MPP+). Neurochem Res. 2015;41(5):1042–9.
28. Legere SA, Haidl ID, Légaré J-F, Marshall JS. Mast cells in Cardiac Fibrosis: New insights Suggest opportunities for intervention. Front Immunol. 2019;10.
29. Weiskirchen R, Meurer SK, Liedtke C, Huber M. Mast cells in liver fibrogenesis. Cells. 2019;8(11).
30. Holdsworth SR, Summers SA. Role of mast cells in Progressive Renal diseases. J Am Soc Nephrol. 2008;19(12):2254–61.
31. Elbasiony E, Cho WJ, Singh A, Mittal SK, Zoukhri D, Chauhan SK. Increased activity of lacrimal gland mast cells are associated with corneal epitheliopathy in aged mice. Npj Aging. 2023;9(1).
32. Blasco MP, Chauhan A, Honarpisheh P, Ahnstedt H, d'Aigle J, Ganesan A et al. Age-dependent involvement of gut mast cells and histamine in post-stroke inflammation. J Neuroinflamm. 2020;17(1).
33. Yamakoshi K, Takahashi A, Hirota F, Nakayama R, Ishimaru N, Kubo Y, et al. Real-time in vivo imaging of p16Ink4a reveals cross talk with p53. J Cell Biol. 2009;186(3):393–407.
34. Schlieve CR, Mojica SG, Holoyda KA, Hou X, Fowler KL et al. Vascular endothelial growth factor (VEGF) bioavailability regulates angiogenesis and intestinal stem and progenitor cell proliferation during postnatal small intestinal development. PLoS ONE. 2016;11(3).
35. Helman A, Klochendler A, Azazmeh N, Gabai Y, Horwitz E, Anzi S, et al. p16Ink4a-induced senescence of pancreatic beta cells enhances insulin secretion. Nat Med. 2016;22(4):412–20.
36. Roa M, Paumet F, Le Mao J, David B, Blank U. Involvement of the ras-like GTPase rab3d in RBL-2H3 mast cell exocytosis following stimulation via high affinity IgE receptors (fc epsilonRI). J Immunol. 1997;159(6):2815–23.
37. Pfirsch-Maisonnas S, Aloulou M, Xu T, Claver J, Kanamaru Y, Tiwari M et al. Inhibitory ITAM Signaling traps activating receptors with the phosphatase SHP-1 to form polarized Inhibisome clusters. Sci Signal. 2011;4(169).
38. Baram D, Adachi R, Medalia O, Tuvim M, Dickey BF, Mekori YA, et al. Synaptotagmin II negatively regulates Ca2+-triggered exocytosis of lysosomes in mast cells. J Exp Med. 1999;189(10):1649–58.
39. Furuno T, Teshima R, Kitani S, Sawada J-i, Nakanishi M. Surface expression of CD63 Antigen (AD1 Antigen) in P815 Mastocytoma cells by transfected IgE receptors. Biochem Biophys Res Commun. 1996;219(3):740–4.
40. Joulia R, Gaudenzio N, Rodrigues M, Lopez J, Blanchard N, Valitutti S et al. Mast cells form antibody-dependent degranulatory synapse for dedicated secretion and defence. Nat Commun. 2015;6(1).
41. López-Otín C, Blasco MA, Partridge L, Serrano M, Kroemer G. Hallmarks of aging: an expanding universe. Cell. 2023;186(2):243–78.
42. Fåhraeus R, Paramio JM, Ball KL, Laín S, Lane DP. Inhibition of pRb phosphorylation and cell-cycle progression by a 20-residue peptide from p16CDKN2/INK4A. Curr Biol. 1996;6(1):84–91.
43. Yousefzadeh MJ, Flores RR, Zhu Y, Schmiechen ZC, Brooks RW, Trussoni CE, et al. An aged immune system drives senescence and ageing of solid organs. Nature. 2021;594(7861):100–5.
44. Yousefzadeh MJ, Zhao J, Bukata C, Wade EA, McGowan SJ, Angelini LA et al. Tissue specificity of senescent cell accumulation during physiologic and accelerated aging of mice. Aging Cell. 2020;19(3).
45. Hudgins AD, Tazearslan C, Tare A, Zhu Y, Huffman D, Suh Y. Age- and tissue-specific expression of senescence biomarkers in mice. Front Genet. 2018;9.
46. Dodig S, Čepelak I, Pavić I. Hallmarks of senescence and aging. Biochemia Med. 2019;29(3):483–97.
47. Buj R, Leon KE, Anguelov MA, Aird KM. Suppression of p16 alleviates the senescence-associated secretory phenotype. Aging. 2021;13(3):3290–312.
48. Papadopoulos EJ, Fitzhugh DJ, Tkaczyk C, Gilfillan AM, Sassetti C, Metcalfe DD, et al. Mast cells migrate, but do not degranulate, in response to fractalkine, a membrane-bound chemokine expressed constitutively in diverse cells of the skin. Eur J Immunol. 2000;30(8):2355–61.
49. Kasakura K, Takahashi K, Itoh T, Hosono A, Nunomura S, Ra C, et al. C/EBPα controls mast cell function. FEBS Lett. 2014;588(24):4645–53.
50. Liu J-Y, Souroullas GP, Diekman BO, Krishnamurthy J, Hall BM, Sorrentino JA et al. Cells exhibiting strong p16INK4a promoter activation in vivo display features of senescence. Proc Nat Acad Sci USA. 2019;116(7):2603–11.
51. Wolff B, Naumann M. INK4 cell cycle inhibitors direct transcriptional inactivation of NF-κB. Oncogene. 1999;18(16):2663–6.
52. Lee M-H, Choi BY, Cho Y-Y, Lee S-Y, Huang Z, Kundu JK et al. Tumor suppressor p16INK4a inhibits cancer cell growth by down-regulating eEF1A2 through a direct interaction. J Cell Sci. 2013;126(Pt 8):1744–52.
53. Tyagi E, Liu B, Li C, Liu T, Rutter J, Grossman D. Loss of p16INK4A stimulates aberrant mitochondrial biogenesis through a CDK4/Rb-independent pathway. Oncotarget. 2017;8(34):55848–62.
54. Safwan-Zaiter H, Wagner N, Wagner K-D. P16INK4A—More than a senescence marker. Life. 2022;12(9).
55. Schwartz LB, Frank Austen K. Enzymes of the mast cell granule. J Invest Dermatology. 1980;74(5):349–53.
56. Freund A, Laberge R-M, Demaria M, Campisi J, Magin TM. Lamin B1 loss is a senescence-associated biomarker. Mol Biol Cell. 2012;23(11):2066–75.
57. Blank U, Huang H, Kawakami T. The high affinity IgE receptor: a signaling update. Curr Opin Immunol. 2021;72:51–8.
58. Munoz I, Danelli L, Claver J, Goudin N, Kurowska M, Madera-Salcedo IK, Huang JD, Fischer A, Gonzalez-Espinosa C, de Saint Basile G, Blank U, Ménasché G. Kinesin-1 controls mast cell degranulation and anaphylaxis through PI3K-dependent recruitment to the granular Slp3/Rab27b complex. J Cell Biol 2016;215(2):203–16
59. Raposo G, Tenza D, Mecheri S, Peronet R, Bonnerot C, Desaymard C. Accumulation of major histocompatibility complex class II molecules in mast cell secretory granules and their release upon degranulation. Mol Biol Cell. 1997;8(12):2631–45.
60. Tharp MD, Seelig LL, Tigelaar RE, Bergstresser PR. Conjugated avidin binds to mast cell granules. J Histochem Cytochemistry. 2017;33(1):27–32.
61. Groot Kormelink T, Arkesteijn GJA, van de Lest CHA, Geerts WJC, Goerdayal SS, Altelaar MAF, et al. Mast cell degranulation is accompanied by the release of a selective subset of extracellular vesicles that contain mast cell–specific proteases. J Immunol. 2016;197(8):3382–92.
62. Vukman KV, Ferencz A, Fehér D, Juhos K, Lőrincz P, Visnovitz T et al. An implanted device enables in vivo monitoring of extracellular vesicle-mediated spread of pro-inflammatory mast cell response in mice. J Extracell Vesicles. 2021;10(1).
63. Crescitelli R, Lässer C, Szabó TG, Kittel A, Eldh M, Dianzani I et al. Distinct RNA profiles in subpopulations of extracellular vesicles: apoptotic bodies, microvesicles and exosomes. J Extracell Vesicles. 2013;2(1).
64. Gunin AG, Kornilova NK, Vasilieva OV, Petrov VV. Age-related changes in Proliferation, the numbers of mast cells, eosinophils, and cd45-Positive cells in human dermis. Journals Gerontol Ser A: Biol Sci Med Sci. 2010;66A(4):385–92.
65. Chatterjee V, Gashev AA. Aging-associated shifts in functional status of mast cells located by adult and aged mesenteric lymphatic vessels. Am J Physiol Heart Circ Physiol. 2012;303(6):H693–702.
66. Grizzi F, Di Caro G, Laghi L, Hermonat P, Mazzola P, Nguyen DD et al. Mast cells and the liver aging process. Immun Ageing. 2013;10(1).
67. Wang RM, Mesfin JM, Karkanitsa M, Ungerleider JL, Zelus E, Zhang Y et al. Immunomodulatory contribution of mast cells to the regenerative biomaterial microenvironment. Npj Regenerative Med. 2023;8(1).
68. Palma AM, Hanes MR, Marshall JS. Mast cell modulation of B cell responses: an under-appreciated Partnership in host defence. Front Immunol. 2021;12.
69. Nakae S, Suto H, Kakurai M, Sedgwick JD, Tsai M, Galli SJ. Mast cells enhance T cell activation: importance of mast cell-derived TNF. Proc Nat Acad Sci USA. 2005;102(18):6467–72.
70. Mitsui Y, Schneider EL. Relationship between cell replication and volume in senescent human diploid fibroblasts. Mech Ageing Dev. 1976;5:45–56.
71. Lengefeld J, Cheng C-W, Maretich P, Blair M, Hagen H, McReynolds MR et al. Cell size is a determinant of stem cell potential during aging. Sci Adv. 2021;7(46).
72. Fingar DC, Salama S, Tsou C, Harlow E, Blenis J. Mammalian cell size is controlled by mTOR and its downstream targets S6K1 and 4EBP1/eIF4E. Genes Dev. 2002;16(12):1472–87.

73. Capellmann S, Sonntag R, Schüler H, Meurer SK, Gan L, Kauffmann M et al. Transformation of primary murine peritoneal mast cells by constitutive KIT activation is accompanied by loss of Cdkn2a/Arf expression. Front Immunol. 2023;14.
74. Gagliardi PA, Puliafito A, di Blasio L, Chianale F, Somale D, Seano G et al. Real-time monitoring of cell protrusion dynamics by impedance responses. Sci Rep. 2015;5(1).
75. Lazki-Hagenbach P, Kleeblatt E, Ali H, Sagi-Eisenberg R. Spatiotemporal patterns of substance P-Bound MRGPRX2 reveal a novel connection between Macropinosome Resolution and secretory granule regeneration in mast cells. Front Immunol. 2022;13.
76. Omari S, Roded A, Eisenberg M, Ali H, Fukuda M, Galli SJ et al. Mast cell secretory granule fusion with amphisomes coordinates their homotypic fusion and release of exosomes. Cell Rep. 2024;43(7).
77. Guerrero-Navarro L, Jansen-Dürr P, Cavinato M. Age-Related Lysosomal Dysfunctions Cells. 2022;11(12).
78. Tan JX, Finkel T. Lysosomes in senescence and aging. EMBO Rep. 2023;24(11).
79. Peters AE, Caban SJ, McLaughlin EA, Roman SD, Bromfield EG, Nixon B et al. The impact of aging on Macroautophagy in the pre-ovulatory mouse oocyte. Front Cell Dev Biology. 2021;9.

Publisher's note